Drug Delivery and Translational Research
https://doi.org/10.1007/s13346-020-00771-y

ORIGINAL ARTICLE

# Perspectives of characterization and bioconjugation of gold nanoparticles and their application in lateral flow immunosensing

Vivek B. Borse[1] · Aditya N. Konwar[1] · Rahul D. Jayant[2] · Pravin O. Patil[3]



## Abstract

Gold nanoparticles (AuNPs) are an important component in the field of biomedical diagnostics. Because of its unique physico-chemical properties, AuNPs have been widely used in biomedical applications such as photothermal cancer therapy, drug delivery, optical imaging, labeling, and biosensing. In this review, we have described synthesis and characterization techniques for AuNPs with recent advancements. Characterization of AuNPs has played an important role in directing its application in various fields and elaborated understanding of its functioning. The characterization techniques used for the analysis of AuNPs utilize its intrinsic properties, such as surface plasmon resonance (SPR) and size-dependent shift in absorption. These properties of AuNPs are furthermore used for the characterization of bioconjugated AuNPs. Surface conjugation of the AuNPs with biomolecules is explored widely for its use in numerous biosensing applications. Biosensor-based diagnostic devices use AuNPs conjugated with a sensing probe for the detection of a specific analyte. AuNPs are also commonly used as a colorimetric sensor in various point-of-care diagnostic techniques. Lateral flow immunosensing (LFIS) technique utilizes AuNPs for the rapid and sensitive detection of various analytes. LFIS is a paper-based detection technique, where the sample containing the analyte flows through the membrane, interacts with immobilized counterparts, and produces results using a detection probe. AuNPs are used as color markers in LFIS, and the presence of an analyte is indicated by the appearance of colored lines on the membrane. The color is a result of the accumulation of AuNP complexes containing the analyte and probe. Effect of characterization parameters of AuNPs on the sensitivity of LFIS, advantages, and disadvantages of using AuNPs for LFIS are discussed concerning the recent reports. Recent applications of AuNPs in LFIS development for the detection of various biomarkers are summarized comprehensively in the table. The review may offer significant insight into the utility of AuNPs for application in the LFIS technique for future development.

**Keywords** Gold nanoparticles (AuNPs) · Characterization · Bioconjugation · Lateral flow immunosensing (LFIS) · Diagnostics

## Introduction

Nanotechnology is a comparatively new field in research which has been emergent since its introduction as a separate but interdisciplinary subject. Nanomaterial has characteristic properties, which are attributed to its small size and quantum effects. Special physical and chemical properties include high surface to volume ratio, different optical properties from their bulk counterparts, surface plasmon resonance, photothermal effects, fluorescence emission, etc. These unique physical and chemical properties of nanomaterial have enabled their use in a variety of applications such as optical imaging, cancer therapeutics, medical diagnostics, and drug delivery as shown in Fig. 1 [1–9]. The nanomaterial is fabricated using a variety of components, among which metal nanoparticles have gained much importance. Gold nanoparticles (AuNPs) have been proved to be useful for imaging, cancer therapy, and drug delivery [10, 11]. AuNPs have been used for the development of electrochemical immunosensors for detection of Zika virus proteins [12]. Iron nanoparticles, i.e., iron oxide nanoparticles, have been used as nanocarriers to encapsulate anti-HIV drugs

✉ Vivek B. Borse
vivek.borse@iitg.ac.in

[1] Centre for Nanotechnology, Indian Institute of Technology Guwahati, Guwahati, Assam 781039, India

[2] Department of Pharmaceutical Sciences, School of Pharmacy, Texas Tech University Health Sciences Center, Amarillo, TX 79106, USA

[3] H. R. Patel Institute of Pharmaceutical Education and Research, Shirpur, Maharashtra 425405, India

Published online: 04 May 2020

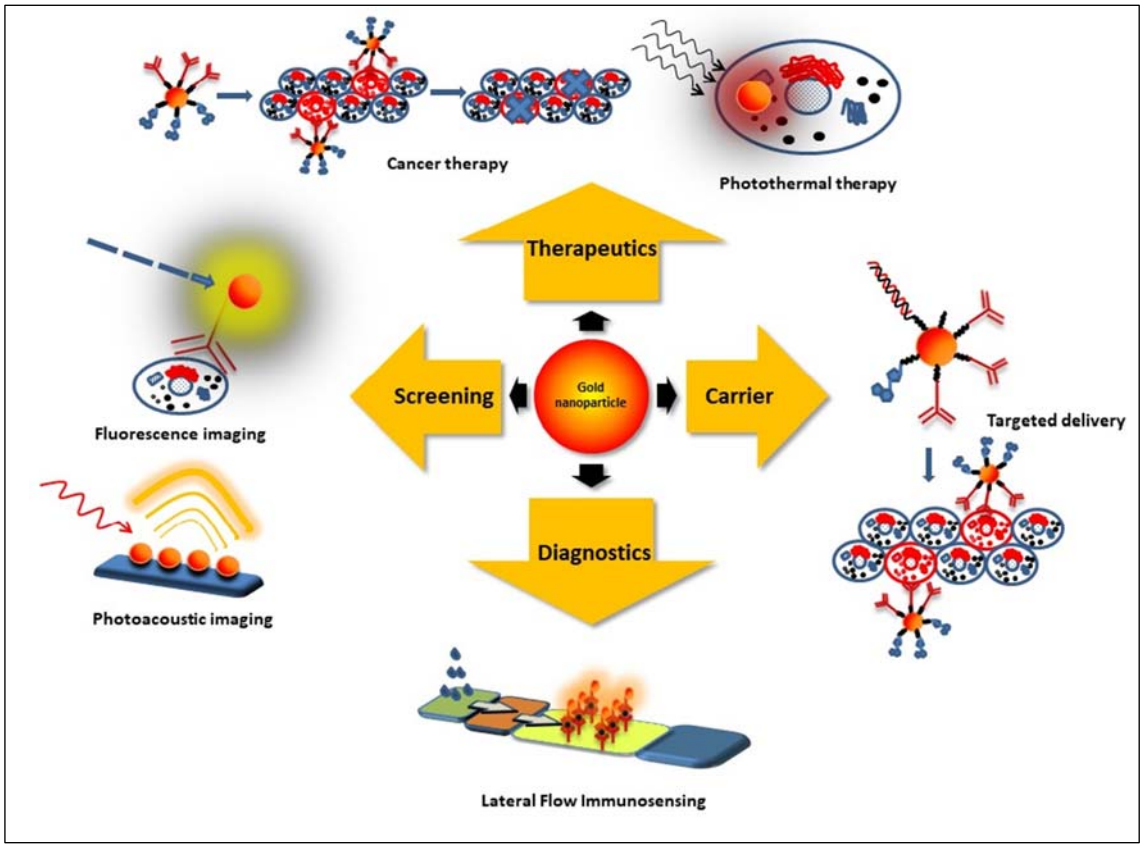


**Fig. 1** Schematic representation of the various applications of gold nanoparticles

for the treatment of nueroAIDS [13]. The antibacterial property of silver metal has been explored in terms of nanoparticles. For example, Banerjee et al. [14] used bimetallic gold-silver core-shell nanoparticles for enhancing the antibacterial activity against several pathogenic microorganisms.

The recent trend in the field of diagnostics has been inclined towards the development of biosensors for rapid detection of diseases or disease-causing agents. Numerous biosensors have been developed using the nanobiotechnology platform. Nanobiosensors are widely used for diagnostics applications such as the detection of allergens in food, toxicants in contaminated water, and antibodies or antigens in blood. The most effective and rapid mode of detection is provided by paper-based biosensors, such as dipstick assays and lateral flow immunoassays (LFIS) [15–17]. The research and development in LFIS and other techniques have led to the evolution of point-of-care (POC) devices in the field of medical diagnostics. These easy-to-use devices are portable and cost-effective, have a low limit of detection, and can be used in resource-limited settings. LFIS is the most widely used POC technique because of a simple methodology and cost-effective large-scale production ability. The well-known forms of simple LFIS are the pregnancy test kit and glucose biosensor, which are abundantly available in any drug store around the world. The prime objective of producing a POC device is to make it effortless, rapid, and having a desirable low limit of detection. All these objectives will be fulfilled if nanotechnology is merged with medical diagnostics.

For the development of POC devices using the LFIS technique, the most commonly used nanomaterial is AuNPs. AuNPs are the preferred choice because of ease of synthesis, optical properties, biocompatibility, bioconjugation ability, etc. Although another nanomaterial, i.e., quantum dots and latex beads, have been used for overcoming some of the limitations shown by AuNPs, AuNPs have been the most widely used nanoparticles for LFIS. Numerous methods have been developed for the synthesis of AuNPs, which can be broadly categorized into chemical [18–21], physical or mechanical [22–24], and biological [25–27] methods of synthesis. Synthesis platform for AuNP is selected in such a way that it reduces its cost and time of preparation, also considering its effectiveness in producing well-shaped and monodispersed particles. Analysis of the synthesized nanoparticles is of importance since the appropriate characterization of the nanoparticles may enable its application in the development of novel nanobiosensor. Along with the advancements in synthesis methods, the characterization of AuNPs has also been improved.

Conjugation of AuNPs with biological molecules (i.e., bioconjugation) enabled its utilization as nanobiosensors. Bioconjugation involves the addition of proteins and nucleic acids on the surface of nanoparticles. The interaction is based on the affinity between the functional groups present on both the interacting entities. The electronic milieu on the surface of the nanoparticle helps to establish non-covalent bonding with the proteins [28]. The non-covalent bonding involves ionic and hydrophobic interactions, while the covalent bonding involves chemisorption, the reaction of functional groups through linkers such as 1-Ethyl-3-[3-dimethylaminopropyl] carbodiimide and *N*-hydroxysuccinimide (EDC-NHS), adapter molecules such as biotin-avidin, and dative bonding [29]. Commonly used techniques for characterization of AuNPs and bioconjugated AuNPs are ultraviolet-visible (UV-Vis) spectroscopy, dynamic light scattering (DLS), zeta potential, Fourier-transform infrared spectroscopy (FTIR), atomic force microscopy (AFM), scanning electron microscopy (SEM), high-resolution transmission electron microscopy (HR-TEM), energy dispersive spectroscopy (EDS), X-ray powder diffraction (XRD), etc. In this review, we have summarized the prominence of using AuNPs in LFIS along with the recent applications and its advantages as well as the limitations. This report also overviews the recent advancements in terms of synthesis methods of AuNPs, bioconjugation methods, and characterization techniques.

## Synthesis and characterization of gold nanoparticles

AuNPs are the most commonly used metallic nanomaterial in the field of biosensing and diagnostics. The unique properties of AuNPs such as surface plasmon resonance (SPR), biocompatibility, and high surface to volume ratio and fluorescence quenching have attracted the attention of researchers for developing devices with high sensitivity and low limit of detection. Over the years, numerous investigations have led to the development of various protocols for the synthesis of AuNPs and their characterization.

### Methods for the synthesis of gold nanoparticles

Several methods have described the synthesis of colloidal AuNPs with a high level of monodispersity. The first report regarding the synthesis of AuNPs was by Faraday in 1857. Subsequently, many techniques have been used to prepare AuNPs with the narrow size distribution. Generally, procedures for the synthesis of AuNPs can be divided into three categories, (1) physical synthesis, (2) chemical synthesis, and (3) biological synthesis.

#### Physical synthesis

Physical methods for synthesis of AuNPs include γ-irradiation, laser ablation, UV-irradiation, microwave irradiation, sonochemical methods, thermolytic process, photochemical process, etc. The physical methods of synthesis offer greater flexibility towards the modification of the surface properties of AuNPs and the controlled synthesis of different sizes of AuNPs. The microwave irradiation method was used to prepare AuNPs of sizes 1–10 nm [24, 30]. The sono-electrochemical method was utilized to prepare the size-controlled synthesis of AuNPs in the size range of 2–15 nm [31]. Among the physical methods, laser ablation is the commonly used method for the synthesis of AuNPs having application in LFIS. Laser ablation has been used as the method for synthesis primarily because of the unique surface chemistry created on the AuNPs reduced with laser-assisted wavelengths. The surface of particles produced by the laser is partially oxidized and acts as electron acceptors. Therefore, these surfaces can easily bind with molecular moieties containing electron donor groups, such as thiols [32]. AuNPs synthesized using laser ablation have been used to develop sensitive biosensor devices using DNA-AuNP conjugates. Zimbone et al. [33] conjugated laser synthesized AuNPs with DNA, mediated by thiol groups, which was characterized using DLS and UV-vis spectroscopy.

#### Chemical synthesis

The most commonly used technique for the synthesis of AuNPs is the chemical reduction of gold chloride using sodium citrate, which was introduced by Turkevich et al. [34] and was further modified by Frens et al. [35]. For this synthesis process, sodium citrate acts both as a reducing agent and a capping agent. Upon reducing the trivalent-gold ($Au^{3+}$) to zero-valent-gold ($Au^{0}$), the citrate ions are adsorbed by the surface of AuNPs and imparting negative charge and stability subsequently. Different sizes of AuNPs are obtained by varying the volume of sodium citrate (1%) [35]. Various reducing agents are used for the synthesis of varying sizes of AuNPs. For example, Rahme et al. [20] have used three different reducing agents to produce AuNPs in the range of 4–150 nm. The smallest particle size (< 10 nm) was obtained using strong reducing agents like sodium borohydride. For particle size of 20–30 nm, the authors have used sodium citrate as the reducing agent, which resulted in particles with high polydispersity. Hydroxylamine-o-sulfonic acid ($NH_2OSO_2OH$) was used as the reducing agent, which produced particles of sizes 40–150 nm.

AuNPs have also been synthesized using the seeded growth method introduced by Brown and Natan [36]. In this method, the dimensions and shape of nanoparticles can be controlled by allowing smaller particles to grow into larger

particles. The AuNPs produced using the seeded growth method are more monodispersed than particles produced by the citrate reduction method. Hydroxylamine ($NH_2OH$) plays a central role in the seeded growth method. It acts as the reducing agent and prevents the production of new nuclei of Au. The surface of AuNPs thus produced are covered with $NH_3OH^-$ groups, which help in the diffusion of $Au^{3+}$ ions on the surface. This causes the formation of larger sized and stable AuNPs coated with $NH_2^-$ groups. Makhsin et al. [21] synthesized AuNPs of sizes 20, 30, and 40 nm with the citrate reduction method and seeded growth method. The AuNPs produced using the seeded growth method were found to be more monodispersed with a lower polydispersity index (PDI; PDI ≤ 0.079) as compared to AuNPs produced using the citrate reduction method (PDI ≤ 0.177). AuNPs of size 4 nm were prepared using sodium borohydride as the reducing agent and was used as the seed. Different volumes of AuNPs seed solution was used to optimize the preparation of AuNPs of size 10 nm. The prepared AuNPs were characterized using UV-vis spectroscopy that showed wavelength maxima at 517 nm [19].

### Biological synthesis

Tremendous improvement has been made in the synthesis methodology of nanoparticles using physical and chemical platforms. Despite the advances made and the advantages that it has to offer, there is a persisting reluctance to use chemical and physical methods of synthesis. This is mostly because of the use of potentially harmful chemicals and extreme physicochemical conditions. Biological synthesis of AuNPs has emerged as a perfect alternative and green approach, making the process implementable, cheaper, and safer [37].

Synthesis using plant and cells/cell-free extracts of microorganisms is the most common method of biosynthesizing AuNPs [25–27]. A simple and rapid method was developed by Noruzi et al. [25], where they used cypress plant extracts and reduced gold salts to obtain AuNPs in room temperatures. The authors found that the average particle size of the AuNPs was dependent on the extract concentration and extract pH. The effect of different parameters on the shape and size of biosynthesized AuNPs was also studied by Kumari et al. [37]. In this study, authors have attempted to understand the effect of temperature, pH of cell-free extract, and the concentration of both the extract and gold salt, on generating different shapes and sizes of AuNPs reduced with fungal cell-free extract of *Trichoderma viride*. It was found that AuNPs of size 3–10 nm had the highest catalytic activity among the other different sized nanoparticles produced by modulating various physical parameters. Baek et al. [38] used *Citrullus lanatus*, i.e., watermelon, which is readily available cheaper source for the synthesis of AuNPs in a size range of 20–140 nm.

Synthesis of AuNPs by fungal species has gained much interest compared to synthesis using bacterial counterparts. This is because most fungal species secrete extracellular enzymes that act as the reducing agent. Ahmad et al. [39] pointed out some advantages of using extracellular enzymes for the synthesis of nanoparticles in solution. The nanoparticles might be immobilized in different matrices or in thin film form, which would not have been possible if the nanoparticles were bound to biomass. The author used a cell-free extract of *Fusarium oxysporum* to produce silver nanoparticles. The protein extracts of *Rhizopus oryzae* were used to synthesize AuNPs of size 5–65 nm and analyzed for their catalytic activity [40]. To reduce metal salts, most of the bacterial species first need to internalize it, which becomes a significant limitation because the bacteria need to be metal tolerant. Biologically synthesized gold nanocomposites were used for biosensing applications. Zhang et al. [41] have used bacterial cellulose (BC) nanofibers as biotemplates for the fabrication of gold nanoparticle-bacteria cellulose (Au-BC) nanocomposites. These Au-BC nanocomposites were used for the development of an $H_2O_2$ biosensor with a low limit of detection.

## Characterization of gold nanoparticles

Over the years, numerous methods have been developed for the synthesis of AuNPs, which are applied in different fields. Depending on the experimental requirements and further applications, the synthesized AuNPs must be appropriately characterized for further use. Characterization of nanoparticles is a complex and critical parameter, in the sense that it cannot be defined by metrics such as chemical composition and concentration. This is because nanoparticles, unlike conventional chemicals, have unique physical and chemical properties that demand exceptional parameters to characterize them. There are two general approaches for the characterization of nanoparticles: spectroscopic method and microscopic method. Spectroscopic methods utilize the physical properties such as electronic behavior on the surface of nanoparticles, which is mostly due to the quantum effects in the nanoscale dimension. Techniques like UV-vis and DLS are commonly used for spectroscopic characterization of nanoparticles. Other spectroscopic techniques include FTIR, nuclear magnetic resonance spectroscopy (NMR), XRD, etc. Microscopic methods, on the other hand, include techniques like AFM, SEM, and HR-TEM. These techniques provide information on the size, morphology, and dispersion state of the nanoparticles and serve as a means of visualizing the nanoparticles.

Spherical AuNPs are the preferentially used nanoparticles for biosensing applications. Their characterization and analysis are crucial for using them as molecular probes for the detection of various biological markers. The commonly used

techniques for characterization of AuNPs are UV-vis spectroscopy, DLS, and zeta-potential. Other high-end techniques like AFM, NMR, FTIR, and HR-TEM were used mostly for characterization of conjugated nanoparticles. There are numerous reports where authors have used a combination of techniques for a comprehensive characterization of AuNPs. UV-vis spectroscopy uses the phenomenon of SPR, which enables the AuNPs to absorb light at a specific wavelength. Also, the absorption peak changes according to the size of nanoparticles. Lou et al. [42] have used UV-vis spectroscopy for the characterization of AuNPs synthesized using the citrate reduction method. Four different sizes of AuNPs of an average diameter of 14, 16, 35, and 38 nm were synthesized and characterized using UV-vis spectroscopy, which showed four different absorption peaks of 519, 522, 528, and 532 nm, respectively [Fig. 2i (A)]. Bioconjugation with antibodies was also analyzed, where a significant red shift was observed in UV spectra when the AuNPs were conjugated with antibodies [Fig. 2i (B)].

Another important technique used for the characterization of nanoparticles is DLS that measures the hydrodynamic diameter of the AuNPs. Zimbone et al. [33] used DLS along with UV-vis spectroscopy to characterize laser-generated AuNPs and found that both the techniques are fast, reliable, and convenient, for analysis of DNA-AuNP conjugation through measurement of their hydrodynamic properties. Zeta potential is used to determine the charge present on the surface of AuNPs. Singh et al. [43] have reported DLS for the characterization of biosynthesized AuNPs. The AuNPs were synthesized using aqueous leaf extracts of macroalgae, *Padina gymnospora*. The hydrodynamic diameter and polydispersity index was measured using DLS. The average diameter was found to be 35.35 ± 0.5 nm with PDI of 0.463 [Fig. 2ii]; zeta potential was found to be − 23.33 ± 1.20 mV.

Besides, these conventional techniques, AFM and HR-TEM, have also been reported for analysis of AuNPs and differentiation between bare AuNPs and antibody-conjugated AuNPs. Tripathi et al. [44] reported HR-TEM and AFM for the characterization of AuNPs and bioconjugated AuNPs. AFM is an excellent tool for analysis of the topography of nanoparticles. It can be used for the visualization of the nanoparticles in a 3D mode that enhances the details regarding the size, shape, and dispersion of nanoparticles. AFM has been used extensively for the study and manipulation of colloidal gold and their functionalization (Fig. 2iii). Malarkodi et al. [45] have reported XRD analysis of eco-friendly synthesized AuNPs. The cubic face-centered AuNP crystal structure was confirmed using XRD, where four

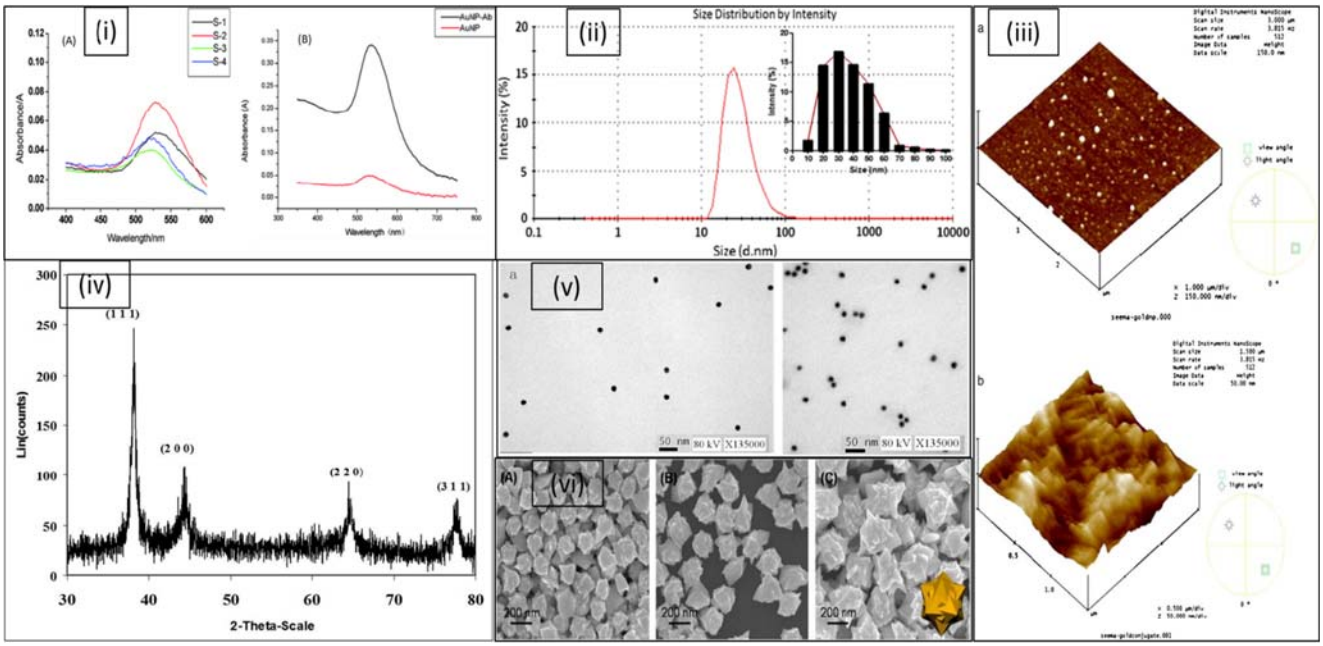


**Fig. 2** Different techniques used for the characterization of AuNPs. **i** UV spectra of non-conjugated and conjugated AuNPs, respectively [Modified and reprinted with permission from (Lou et al., 2012) [42], Copyright 2012, Royal Society of Chemistry]. **ii** Size distribution pattern in DLS 5 [Reprinted with permission from (Singh et al., 2014) [43], Copyright 2014, Springer]. **iii** Shows surface analysis of AuNPs and conjugated AuNPs by AFM [Reprinted with permission from (Tripathi et al., 2012) [44], Copyright 2012, Elsevier]. **iv** Shows the XRD spectra of AuNPs with four different peaks at 38.2°, 44.7°, 64.5°, and 78.3° indexed at planes of (111), (200), (220), and (311) confirming the crystal structure of AuNPs [Reprinted with permission from (Malarkodi et al., 2013) [45], Copyright 2013, Malarkodi et al.]. **v** Shows the TEM images of AuNPs and conjugated AuNPs [Reprinted with permission from (Wang et al., 2014) [46], Copyright 2014, Plos one]. **vi** Shows FE-SEM images of synthesized tipped flowerlike AuNPs using different volumes of AuNP seeds (20 nm), (A) 0.13 ml, (B) 0.07 ml, and (C) 0.02 ml [Reprinted with permission from (Zhang et al., 2015) [47], Copyright 2015, American Chemical Society]

prominent peaks were present at 38.2°, 44.7°, 64.5°, and 78.3° indexed as planes (111), (200), (220), and (311), respectively (Fig. 2iv).

TEM analysis was used as a conventional characterization technique for AuNPs by Wang et al. [46] (Fig. 2v). It is a type of electron microscopy in which the electron beams are transmitted across the sample to form the image instead of reflecting against the surface of the sample as in the case of SEM. It is an excellent tool for determining the average diameter of AuNPs. Chandra et al. [48] used TEM for the measurement of the average diameter of AuNPs, which were used for the fabrication of an electrochemical biosensor for the detection of multidrug-resistant cancer cells in biological matrixes. Taranova et al. [49] used TEM along with DLS to characterize AuNPs and their conjugates. In another work, scanning-TEM (STEM) along with energy-dispersive X-ray spectroscopy (EDS) and electron diffraction techniques has been used for the characterization of nano-drug carriers [50]. SEM has also been used for the surface studies of AuNPs. FE-SEM provides topographical and detailed information at a higher magnification and resolution. It provides a better depth of field compared to conventional SEM. Zhu et al. [51] used SEM for analysis of self-assembled bis(2-thienyl)-1H-pyrrole-1-(p-benzoic acid) (DPB) on AuNPs and hydrazine-AuNP-aptamer bioconjugates. The authors developed an electrochemical biosensor for the detection of breast cancer cells. Wang et al. [52] used SEM analysis for the morphological study of the formation of Au-Ag hollow nanoparticles. Zhang et al. [47] used FE-SEM along with TEM and UV-vis spectroscopy for characterization of flower-like AuNPs (Fig. 2vi).

## Bioconjugation of gold nanoparticles

In the field of biosensors and diagnostics, where nanoparticles are used as probes, the nanoparticles are functionalized/conjugated with a biological molecule. In the LFIS techniques, the nanoparticles are conjugated with a detection molecule, which binds with the analyte and a capture molecule immobilized in the test zone detects this complex. To improve the sensitivity of the assay, multiplex LFIS was developed for the detection of multiple analytes in the same strip [53, 54]. This is achieved through conjugation of antibodies against their specific analytes to the nanoparticles and their simultaneous detection in the test zone.

### Bioconjugation techniques and its mechanism

Bioconjugation involves an interaction of chemical/functional groups from nanoparticle and the biomolecule. The interaction may be physical or chemical, depending on the type of molecules used. These interactions of nanoparticles with the biomolecules may be enhanced by incorporating different functional groups or ligands to the interacting surface. This increases the stability of the interaction. He et al. [55] reported conjugation of thiolated DNA to AuNPs surface, where sodium dodecyl sulfate (SDS) was used to enhance the interaction. Thiolated DNA was used for conjugation with laser-produced AuNPs. These laser-produced AuNPs provided electrostatically stable and oxidized surfaces, which aided the attachment of thiol groups [33]. Polyethylene glycol (PEG) is also reported to be conjugated onto AuNPs [56]. The introduction of PEG increases the biocompatibility and stability of the nanoparticles. It also prevents the nanoparticles from aggregation in solution, thus acting as a capping agent. Polymers are also reported to be conjugated with AuNPs, where the terminal group of the polymer was reduced to a thiol and mixed with AuNPs to prepare glycopolymer-substituted AuNPs [57]. Since most of the analytes are of protein origin, the production of antibodies against them is a necessary step. There are numerous reports where antibodies or antigens are conjugated to AuNPs for the development of LFIS. Antibodies are the most commonly used biomolecule for conjugation with AuNPs. For the detection of a particular analyte, specific antibodies against them are selected, which are bound to the AuNPs as the detection probe. For example, the anti-clenbuterol antibody was conjugated with Au-Ag hollow nanoparticles for the detection of clenbuterol [52]. In another work, monoclonal antibodies against cytomegalovirus were conjugated with AuNPs as the detection probe [58]. Alternatively, in the case of some infectious diseases, the antibodies, which are produced by our body, become the target analyte. In these cases, the antigens, which are specific for the antibodies, are conjugated with the AuNPs as the detection probes. For the detection of the human tetanus antibody in blood serum, tetanus antigen conjugated with AuNPs was used [59]. Immunoglobulins against *Treponema pallidum* were detected using TPN17 and TPN47 antigen, which were conjugated to AuNPs [60]. Antibodies and other functionalized groups are adsorbed on the nanoparticles surface non-specifically through electrostatic interaction between the negatively charged nanoparticle surface and the positively charged amino acids at a specific pH. Antibodies are conjugated to nanoparticles through non-covalent interactions such as hydrophobic interaction and ionic interactions and dative bonding. The electrical double layer (EDL) is a characteristic feature of colloidal nanoparticle suspensions. During conjugation of antibodies with AuNPs, this EDL plays a vital role in the interaction. This double layer consists of two parallel layers of ions (Fig. 3). The first layer coincides with the surface of the nanoparticle and corresponds to the surface charge of the nanoparticles (which is mostly negative). The second layer is in the fluid and electrically screens the first layer. The EDL results in the production of other electrical layers around the nanoparticle surface, such as a diffuse layer, stern layer, and slipping plane. The interaction

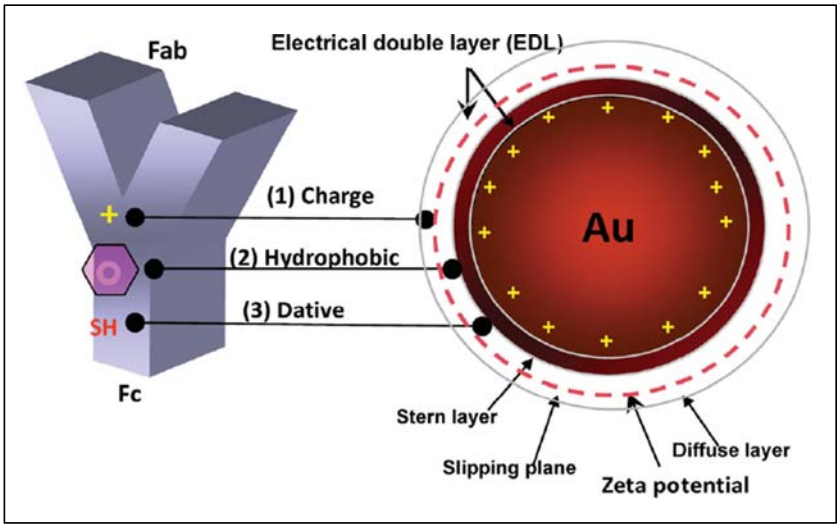


**Fig. 3** Schematic representation of chemical binding principle for bioconjugation of AuNPs [Reprinted with permission from (Chou, 2013) [28], Copyright 2013, Royal Society of Chemistry]

between all these electrically charged layers and the charges present in the antibody surface results in the successful conjugation [28].

For covalent conjugation of antibodies to the surface of AuNPs, researchers have used various linkers such as a biotin-avidin linker and EDC-NHS linker. The anti-HER2 antibody was conjugated with AuNPs through a PEG-linker [orthopyridyl disulfide-polyethyleneglycol-*N*-hydroxysuccinimide (OPSS-PEG-NHS)], which was attached to the surface of nanoparticle through a sulfur-containing group at the PEG linker [61]. Similarly, EDC is also used as a linker for attaching proteins to the surface of nanoparticles [62]. Biotin-avidin linkage is another covalent conjugation method for binding biological molecules to the surface of nanoparticles. The avidin ligands are functionalized onto the nanoparticle surface for providing ample functional groups so that the molecules with biotin can bind with a stable interaction [63].

## Characterization techniques for bioconjugation

Bioconjugated nanoparticles form the basis of the development of sensitive probes that are employed in immunosensing. The stability and biocompatibility of these conjugates are important parameters, which have to be taken into consideration while developing a biosensor. Therefore, characterization techniques are important concerning synthesis as well as bioconjugation of AuNPs; schematics are shown in Fig. 4. The characterization of bioconjugated nanoparticles is crucial for its further application as detection probes in LFIS. The prepared bioconjugates need to be stable and efficient for interacting with other biological molecules. During conjugation, the surface properties, along with the inherent biological properties of the conjugate, should be conserved and analyzed simultaneously.

UV-vis spectroscopy is a conventional technique used for the determination of bioconjugation. Here, the change in the absorption peak is detected when the nanoparticles are adsorbed with proteins or other biomolecules. Bioconjugation changes the oscillation pattern of the conduction band electrons in a similar way as increasing the size of the nanoparticle. The red shift after conjugation of the nanoparticles with proteins is due to the surface modification of the nanoparticle with a layer of protein. This layer alters the refractive index of the surface of the embedding medium [64, 65]. Also, during covalent bonding with either nucleic acid or protein, the thiol groups or the thiol-gold bond perturbs the conduction electron cloud in the particle. The reduced electron density reduces the plasmon frequency or increases the plasmon wavelength resulting in the red shift [66].

DLS is a useful tool for measuring the hydrodynamic diameter of the nanoparticles. The slight increase in the size of the AuNPs is detected, which confirms the successful conjugation. Rahme et al. [20] used DLS for confirming the functionalization of AuNPs with PEG and also its conjugation with antibodies by monitoring the increase in hydrodynamic diameter of AuNPs. FTIR is an excellent tool for analyzing the interaction between antibodies and nanoparticle surface. The IR spectra give peaks at particular wavenumbers corresponding to the specific functional groups present on the analytes. Therefore, by observing the presence or absence of functional groups such as N–H, O–H, or C=O, conclusions can be drawn on the interaction between nanoparticle surface and antibodies. For example, the peaks at wavenumbers of 3300 $cm^{-1}$ and 1645 $cm^{-1}$ in IR spectra represented the O–H and C=O groups, which are the characteristic functional groups present on citrate-stabilized gold particles, while the melamine antibodies also gave characteristic peaks for N–H, C=S, and N=O, which confirmed the presence of antibodies. Further, when peaks for AuNP-antimel were observed, no new peaks were generated, and also the decreased transmittance in all the

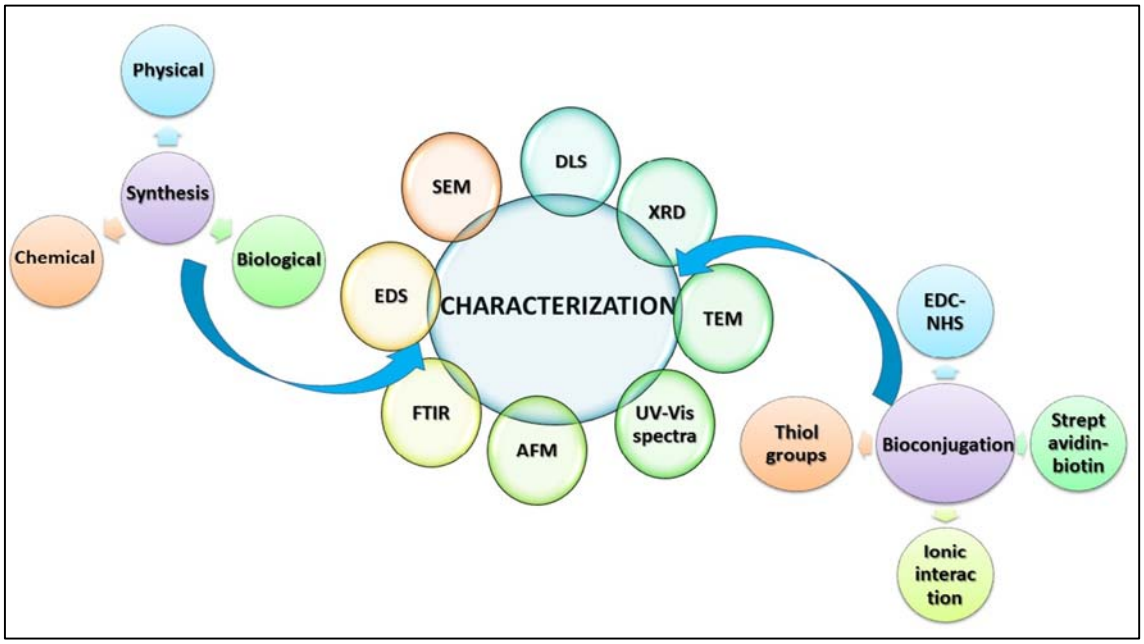


**Fig. 4** Schematic representation of synthesis and bioconjugation methods and techniques used for characterization

peaks indicated that no bonds were formed between AuNPs and anti-melamine, i.e., the antibodies were electrostatically covered over the nanoparticle surface [67]. Lou et al. [42] also used FTIR for the characterization of bioconjugation. The peaks corresponding to C=O stretching and O–H deformation were characteristics of citrate-synthesized AuNP. It was found that after antibody conjugation, O–H, C=O, and several other N–H deformation peaks disappeared, confirming the successful interaction of the protein with the nanoparticle surface.

Lou et al. [42] used EDS data to show that the antibody is loaded onto the AuNPs. The spectra showed an S energy spectrum at the AuNPs after conjugation with antibodies. The small S-peak comes from the sulfur-containing amino acid residues in the proteins. The presence of this peak confirms the loading of antibodies onto the nanoparticles. Tripathi et al. [44] also used AFM surface topography for characterizing the bioconjugated AuNPs and analyzed their surface morphologies in 3D; results are shown in Fig. 2iii. The analysis showed that the root-mean-square of the roughness was less for AuNPs (1.384 nm) compared to conjugated AuNPs (7.861 nm). This increased roughness represented the conjugation of antibodies onto the surface of nanoparticles. Nara et al. [68] also used AFM for the roughness analysis of conjugated and non-conjugated AuNPs. Lou et al. [42] used TEM for visualizing four different antibody-gold conjugates. The presence of a thin layer of low electron density was observed around the nanoparticle representing the conjugated antibodies. The thickness of the layer was determined to be 4 nm, which corresponded with the size of the conjugated immunoglobulins. The confirmation of conjugation is provided by a presence of halo zone with low electron density around the AuNPs (shown in Fig. 2v), which is compared with the non-conjugated AuNPs [46].

Almost all the characterization techniques utilize the different properties such as size, shape, and surface features between non-conjugated and conjugated AuNPs to confirm the effective binding of the biological molecules to the AuNPs. Although several reports are elucidating the characterization of bioconjugation, there is a lack of data showing the difference in the size of conjugated AuNPs compared to non-conjugated AuNPs, when it comes to the various reports of the development of LFIS. This inadequacy of data representation needs to be overcome for building a better and comprehensive report on LFIS. For example, when TEM is used for the analysis of conjugation, a clear difference in size should be mentioned along with the observation of the halo zone of antibodies around AuNPs. This will be helpful in better understanding of the result and will clearly show the outcome of conjugation or functionalization. Moreover, an additional characterization technique such as SDS PAGE, which has been used by Borse et al. [69], for bioconjugation of quantum dots, may show the way for a thorough analysis of AuNPs conjugation.

## Gold nanoparticles for lateral flow immunosensing

Colloidal AuNPs are the most common choice of the nanoparticles for LFIS. LFIS technique is based on immunological reactions where an antigen is detected by specific antibody tagged with various markers such as AuNPs, latex beads,

carbon dots, and quantum dots. Depending on the detection type, the LFIS is categorized in the qualitative, semi-quantitative, and quantitative methods [70–72]. LFIS has become an indispensable method in the field of diagnostics, which exhibits a low limit of detection, high sensitivity, high specificity, robustness, low cost, etc. The AuNPs are synthesized as a colloidal gold solution containing monodispersed and well-defined spherical AuNPs. Studies have been performed where AuNPs as colloidal gold solutions were used for the development of lateral flow devices or immunochromatographic strips to detect a variety of compounds and enzymes. Colloidal gold was conjugated with different types of detection probes (either antigen or antibodies) to detect various analytes like immunoglobulin G (IgG) against *Treponema pallidum* [60], enzymes like microbial transglutaminase (MTGase) in frozen food samples [73], cortisol in human serum [68], *Staphylococcus aureus* in food samples [74], human serum albumin in urine samples for diagnosis of microalbuminuria [75], and nitrofuran metabolites in fish samples [53]. The detection of the analytes was carried out using AuNPs of varying sizes. The variation in sizes of AuNPs has a profound effect on the sensitivity of LFIS and affects the conjugation efficiencies. Thus, controlling the size and shape of synthesized AuNPs becomes an essential parameter for increasing the efficiency of bioconjugation and for increasing the sensitivity of detection of LFIS.

## Size and shape of gold nanoparticles

The colloidal AuNPs are synthesized in varying sizes, depending on its application. AuNPs of size between 20 and 50 nm are most commonly used for LFIS; besides many authors have reported the use of smaller sized AuNPs, e. g., 10–15 nm [19, 59, 76–78]. AuNPs with an average diameter of 40 nm provided excellent surface properties and low steric hindrance, which are ideal to be used for bioconjugation [79]. The effect of change in the size of AuNPs on the conjugation efficiency and sensitivity of LFIS has been studied earlier [42]. Four different sizes of AuNPs were prepared (i.e., 14 nm, 16 nm, 35 nm, and 38 nm) and conjugated with monoclonal antibodies that are specific for the detection of hepatitis B virus surface antigens. It was found that AuNPs having a size of 16 nm were more efficient for conjugation, as it required a minimum concentration of antibodies that also prevented aggregation. However, the detection sensitivity was lower than that of the AuNPs of size 38 nm. Rahme et al. [20] have used various reducing agents to obtain different sizes of AuNPs, which affect the efficiency of bioconjugation. The weak reducing agent, i.e., hydroxylamine-o-sulfonic acid ($NH_2OSO_2OH$), was used to prepare AuNPs of 60, 90, and 150 nm, whereas very small-sized AuNPs (i.e., 4 nm) were prepared using two relatively stronger reducing agents such as sodium citrate and sodium borohydride. Bioconjugation of apolipoprotein E and bovine serum albumin (BSA) was performed successfully with AuNPs of sizes 15 nm, 30 nm, and 90 nm. Colorimetric biosensors were also developed using AuNPs to detect thrombin and fibrinogen in human blood samples [80]. Three different sizes of AuNPs were prepared, i.e., 13 nm, 32 nm, and 56 nm. The sensitivity of AuNPs of size 56 nm was found to be lower because of its large size and reduced stability due to steric hindrance during conjugation. On the other hand, higher sensitivity was obtained for the AuNPs of size 13 nm due to a smaller size and high aggregation capacity.

Depending on the experimental requirements, different shapes of AuNPs have been used along with variations in sizes. Petrakova et al. [81] have used gold nanoflowers along with gold nanospheres to develop a bicolor test zone in the lateral flow strip. The gold nanoflowers of sizes 43, 44, 68, 65, 76, and 89 nm showed blue color upon aggregation, and gold nanospheres of sizes 73 and 75 nm showed characteristic red color in the detection zone of the strip. In another study, hierarchical flower-like AuNPs were prepared to detect *E.coli* O157:H7. Using a one-step process, three types of flower-like AuNPs were prepared, such as tipped flower-like, popcorn-like, and large-sized flower-like AuNPs [47]. After the three types were compared for sensitivity, tipped flower-like AuNPs exhibited high sensitivity for the detection of *E.coli* O157:H7. The use of surface-enhanced Raman scattering (SERS) based flower-like gold-silver core-shell bimetallic nanoparticles has also been reported to detect β-adrenergic agonist brombuterol in swine meat and urine samples [82]. Optical DNA biosensor was developed for the detection of *Chlamydia trachomatis* pathogen with the use of gold nanorods (GNRs) as the molecular probes [83]. Thus, the size and the shape of AuNPs are considered important factors in determining the sensitivity of LFIS. Optimization of particle size and shape is required to overcome the challenges regarding the sensitivity of LFIS.

## Advantages of using AuNPs for LFIS

Among the group of noble metals, AuNPs are commonly used as the detection marker for biosensing applications. This is due to the unique physical, chemical, and optical properties of AuNPs, along with relative ease of preparation and manipulation. The most interesting property is the surface behavior of AuNPs. AuNPs exhibit the SPR phenomenon, where the oscillation of electrons in the conduction band causes a specific absorption peak when irradiated with visible light. Depending on SPR, the characteristic red color of AuNPs forms the basis of detection while using lateral flow biosensor devices. The SPR phenomenon is strongly dependent on the dielectric constant of the environment, along with the shape and size of nanoparticles [84]. This environmental dependency represents a significant advantage in biosensing

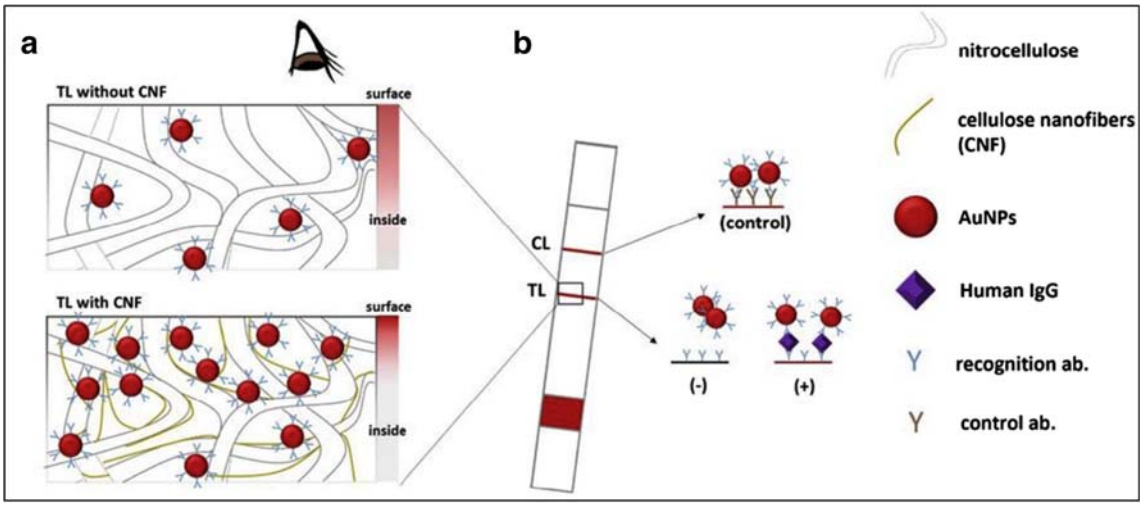


**Fig. 5** Schematic illustration of signal enhancement strategy using carbon nanofibers (CNF) in the paper strip. (A) The surface of the test line has more aggregated AuNPs due to the introduction of CNF. (B) Position of test line (TL) and control line (CL) on the strip [Reprinted with permission from (Quesada-González et al., 2019) [92], Copyright 2019, Elsevier]

applications. The change in electron density or the oscillation frequency results in color change as well as a change in the absorption wavelength that can be detected by employing techniques and instruments such as UV-vis spectrometry and DLS. Fluorescence quenching is another property of gold nanoparticle that is used for immunoassays. Due to the phenomenon called Forster resonance energy transfer (FRET) from donors to acceptors, there is fluorescence quenching of the fluorescent probe, and this phenomenon has been used to develop immunosensing methods using molecular acceptors in sandwich ELISA format. However, the energy transfer efficiency reduces when the distance between the acceptor and donor is greater than 5–7 nm. Since the distance of acceptor and donor in conjugated protein-antibody complexes is larger than 10 nm, the efficiency of energy transfer is limited. The use of gold nanoparticles in these fluorescence quenching techniques was found to be very effective [85]. The high efficiency of fluorescence quenching by AuNPs is due to a smaller size, because of which, the energy transfer takes place easily. Also, since AuNPs have no defined direction of the dipole, the energy transfer can take place in any orientation of the donor relative to the surface of AuNP.

AuNPs can be tuned or modified with ease, which facilitates its use as an excellent material for bioconjugation. The spherical AuNPs have a high surface to volume ratio due to which adsorption of the biomaterial becomes feasible. Also, functionalization of the particle surface with streptavidin or biotin has been found to improve the conjugation efficiencies along with the increase in sensitivity of LFIS [86]. The sensitivity of the lateral flow assay was also improved by

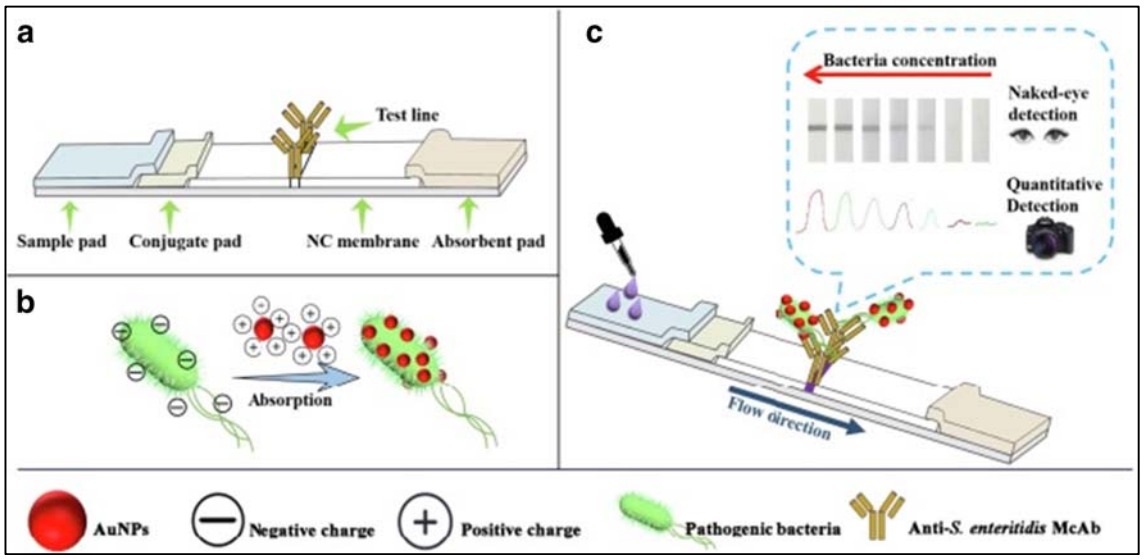


**Fig. 6** Schematic representation of a label-free strategy for the detection of foodborne pathogens using positively charged AuNPs. [Reprinted with permission from (Bu et al., 2019) [93], Copyright 2019, Elsevier]

**Table 1** Application of gold nanoparticles-based LFIS in human and animal healthcare

| Sr. no. | Type of gold nanoparticle (AuNP) | Size of AuNPs | Characterization techniques for AuNPs | Type of conjugation material | Technique used for conjugation |
|---|---|---|---|---|---|
| 1 | Colloidal AuNPs | 20 nm | NA | Detection: monoclonal antibody against human cytomegalovirus Capture: goat anti-mouse IgG | Incubation of mAb CMV with colloidal AuNPs and addition of NaCl followed by centrifugation |
| 2 | Colloidal AuNPs | 20 nm | NA | Detection: monoclonal antibody anti-GPV Capture: anti-GPV polyclonal antibody | Mixing of mAb anti-GPV with AuNP in an optimum pH and concentration followed by centrifugation, suspension of pellet in citrate buffer containing BSA |
| 3 | Four different sizes of AuNPs | 14 nm, 16 nm, 35 nm, 38 nm | UV-vis spectroscopy, DLS, and TEM | Detection: anti-HBsAg mAb 1 Capture: anti-HBsAg mAb 2 | Mixing of anti-HBsAg mAb 1 with AuNP in an optimum pH and concentration followed by centrifugation. The pellet was suspended in Tris buffer containing BSA and 10% sucrose |
| 4 | Colloidal AuNPs | 20 nm | UV-vis spectroscopy and TEM | Detection: mAb(anti-GroeL) MAb 1G2F10 Capture: MAb 1G2F10 | Mixing of mAb (anti-GroeL) with AuNP in an optimum pH and concentration followed by centrifugation. The pellet was suspended in Tris-HCl buffer |
| 5 | AuNPs | 30–40 nm | UV-vis spectroscopy and TEM | Detection: DNA oligomers and Raman reporter MGITC (malachite green isothiocyanate) streptavidin-biotinylated Capture: streptavidin-biotinylated capture DNA | Thiolated DNAs were conjugated on the surface of MGITC-functionalized AuNPs |
| 6 | Colloidal AuNPs | 13 nm | UV-vis spectroscopy and TEM | Detection: tetanus antigen Capture: tetanus antigen | Mixing of tetanus antigen (Ag) with AuNP in an optimum pH and concentration followed by centrifugation |
| 7 | AuNPs synthesized using a seeded growth method | 10 nm | UV-vis spectroscopy and TEM | Detection: goat anti-human IgA Capture: human IgA | Mixing of goat anti-human IgA with AuNPs in an optimum pH and concentration followed by centrifugation |
| 8 | Gold nanospheres and gold nanoflowers | Different sizes and shapes of AuNPs | UV-vis spectroscopy, DLS, and TEM | Detection: streptavidin and IgG antibodies Capture: T2T-BSA and biotin-BSA | Mixing of IgG antibodies with AuNP in an optimum pH and concentration followed by centrifugation |
| 9 | Colloidal AuNPs | 25 nm | UV-vis spectroscopy | Detection: antibodies against snake venom (ASVA) Capture: species-specific Ab | Mixing of anti-ASVA with AuNP in an optimum pH and concentration followed by centrifugation |
| 10 | Gold nanoparticles (GNP) | 30 nm | UV-vis spectroscopy | Detection: anti-mycotoxin deoxynivalenol Capture: anti-mycotoxin deoxynivalenol | Mixing of anti-DON with AuNP in an optimum pH and concentration followed by centrifugation. Conjugated AuNPs were resuspended in Tris buffer that contained TBSA (1%BSA, 1% sucrose, and 0.05% sodium azide) |
| 11 | Colloidal AuNPs | 13–21 nm | UV-vis spectroscopy, TEM, and DLS | Detection: polyclonal antibodies against Trypanosoma (anti-horse-IgG) Capture: antigen-specific to *Trypanosoma* | Mixing of anti-horse-IgG with AuNP in an optimum pH and concentration followed by centrifugation. The pellet was resuspended in 10mMphosphate buffer containing 0.1% BSA, pH 7.2 |
| 12 | Colloidal AuNPs synthesized using different reducing agents | Different sizes of AuNPs, ranging from 4 to 140 nm | UV-vis spectroscopy, TEM, DLS, and zeta analyzer. | Detection: ApoE antigen and BSA Capture: ApoE antigen | Mixing of ApoE antigen with AuNP in an optimum pH and concentration followed by centrifugation. The binding of the protein to the nanoparticle was through an amide linkage, which was due to the PEGylation of the surface of nanoparticles. The PEGylation gave the nanoparticle surface the −SH ligands for the amide linkage to proteins |
| 13 | Colloidal AuNPs | 15 nm | | | |

**Table 1** (continued)

| | | | | | |
|---|---|---|---|---|---|
| | | | UV-vis spectroscopy and TEM | Detection: monoclonal antibodies against olaquindox Capture: monoclonal antibodies against olaquindox | Mixing of mAb with AuNP in an optimum pH and concentration followed by centrifugation. The pellet was resuspended in PBST – phosphate-buffered saline with Tween20 |
| 14 | Colloidal AuNPs | 20 nm | UV-vis spectroscopy | Detection: recombinant protein (antigen NS1) Capture: anti-NS1 | Mixing of antigen NS1 with AuNP in an optimum pH and concentration and followed by centrifugation |
| 15 | Spherical AuNPs | 13 nm, 32 nm, 56 nm | UV-vis spectra, SPR, and TEM | Detection: coagulation related protein thrombin (Thr-Au) | Mixing of thrombin protein with AuNP solution in a specific pH. Conjugation occurred due to electrostatic interaction |
| 16 | Colloidal AuNPs | 40 nm | UV-vis spectra and TEM | Detection: avidin-biotin functionalized AuNP conjugated with antibodies against *E.coli* O157:H7 Capture: antibodies against *E.coli* O157:H7 | Mixing of anti-O157:H7 with AuNP in an optimum pH and concentration followed by centrifugation. Biotin was added along with streptavidin-HRP |
| 17 | Colloidal AuNPs (purchased) | 10 and 40 nm | UV-vis spectra | Detection: two conjugates, 1st with anti-troponin 1 antibody and the 2nd with anti-BSA Capture: anti-troponin 1 | Mixing of anti-troponin 1 with AuNP in an optimum pH and concentration followed by centrifugation |
| 18 | Colloidal AuNPs | 25 nm | NA | Detection: anti-IFNg mAbs Capture: anti-IFNg pAbs | Mixing of anti-IFNg mAbs with AuNP in an optimum pH and concentration followed by centrifugation |
| 19 | Colloidal AuNPs | 20 nm | DLS, UV-vis spectra and fluorescence spectroscopy | Detection: mouse anti-bacterial transglutaminase antibody (monoclonal antibody) Capture: rabbit anti-bacterial-transglutaminase antibody (polyclonal antibody) | Mixing of anti-bacterial transglutaminase with AuNP in an optimum pH and concentration followed by centrifugation |
| 20 | Colloidal AuNPs | 15 nm | UV-vis spectra | Detection: nucleic acid streptavidin HRP Capture: biotinylated capture nucleic acid | Thiolated DNAs were conjugated on the surface of HRP-functionalized AuNPs |
| 21 | Colloidal AuNPs | 15 nm | UV-vis spectra and TEM | Detection: staphylococcal protein A Capture: *T. gondii*-specific recombinant proteins | Mixing of staphylococcal protein A with AuNP in an optimum pH and concentration followed by centrifugation |
| 22 | Colloidal AuNPs | 40 nm | UV-vis spectra and TEM | Detection: anti-NDV-6C4 monoclonal antibody Capture: anti-NDV-4D9 monoclonal antibody | Mixing of anti-NDV-6C4 mAb with AuNP in an optimum pH and concentration followed by centrifugation |
| 23 | Colloidal AuNPs | 25 nm | UV-vis spectra and TEM | Detection: recombinant protein TPN17 and TPN47 Capture: monoclonal antibody to the human γ chain-specific IgG | Mixing of protein TPN17 with AuNP in an optimum pH and concentration followed by centrifugation |
| 24 | Colloidal AuNPs | 20 nm | UV-vis spectra and TEM | Detection: monoclonal antibodies anti-Cr-EDTA McAb Capture: antigen Cr-EDTA-BSA | Mixing of anti-Cr-EDTA with AuNP in an optimum pH and concentration followed by centrifugation |
| 25 | Different sizes of colloidal AuNPs | 20 nm, 30 nm, 40 nm | UV-vis spectra, DLS, and TEM | Detection: mouse anti-human IgG4 (MαHIgG4) Capture: B*m*R1 recombinant antigen | Mixing of anti-human IgG4 with AuNP in an optimum pH and concentration followed by centrifugation |
| 26 | Colloidal AuNPs | 24 nm | UV-vis spectra and TEM | Detection: monoclonal antibodies to IL-6 and TNFα Capture: polyclonal antibodies to IL-6 and TNFα | Mixing of antibodies to IL-6 and TNFα with AuNP in an optimum pH and concentration followed by centrifugation |
| 27 | Colloidal AuNPs | 40 nm | UV-vis spectra, TEM, and SPR | Detection: monoclonal antibodies (MTB 38 kDa monoclonal antibody) Capture: MTB6–14–38 kDa fusion antigen | Mixing of MTB 38 kDa monoclonal antibody with AuNP in an optimum pH and concentration followed by centrifugation |
| 28 | Colloidal AuNPs | 20 nm | TEM | Detection: polyclonal antibodies against *Mycoplasma suis* Capture: polyclonal antibodies against *Mycoplasma suis* | Mixing of polyclonal antibodies against *Mycoplasma suis* with AuNP in an optimum pH and concentration followed by centrifugation |
| 29 | Colloidal AuNPs | 36 nm | DLS, SPR, AFM, HR-TEM | Detection: antigen F-3-CMO-ADH-BSA Capture: antibody anti-cortisol antibody raised against F-3-CMO–BSA immunogen | Mixing of Antigen F-3-CMO-ADH-BSA with AuNP in an optimum pH and concentration followed by centrifugation |
| 30 | Colloidal AuNPs | 20 nm | UV-vis spectroscopy, | | Mixing of anti-*Staphylococcus aureus* antibody with AuNP in an optimum pH and concentration followed by centrifugation |

**Table 1** (continued)

| | | | | | |
|---|---|---|---|---|---|
| | | | DLS, and TEM | Detection: mouse anti-*Staphylococcus aureus* antibody Capture: mouse anti-*Staphylococcus aureus* antibody | |
| 31 | Colloidal AuNPs | 20 nm | UV-vis spectroscopy | Detection: monoclonal antibodies MAb EMRC1 Capture: human serum albumin (HSA) antigen | Mixing of MAb EMRC1 with AuNP in an optimum pH and concentration followed by centrifugation |
| 32 | Colloidal AuNPs | 20 nm | UV-vis spectra and TEM | Detection: human IgG Capture: anti-human IgG | Mixing of human IgG with AuNP in an optimum pH and concentration followed by centrifugation |
| 33 | Colloidal AuNPs | 15 nm | UV-vis spectra and TEM | Detection: antibody of *S. Typhi* O901 Capture: antibody of *S. Typhi* O901 | Mixing of the antibody *of S. Typhi* O901 with AuNP at an optimum pH and concentration followed by centrifugation |
| 34 | Polymer modified AuNPs | 40 nm | UV-vis spectroscopy, DLS, and TEM | Detection: terminally thiolated poly(Man-r-AAm) Capture: rabbit anti-ConA antibody | Terminally thiolated poly(Man-r-AAm) was mixed with an aqueous dispersion of AuNPs and then purified by dialysis with Milli-Q water |
| 35 | Colloidal AuNPs | 36 nm | UV-vis spectroscopy, DLS, HR-TEM, and AFM | Detection: 17-α-hydroxyprogesterone-3-carboxymethyl-bovine serum albumin immunogen Capture: antibody against the detection immunogen | Mixing of 17-α-hydroxyprogesterone-3-carboxymethyl-bovine serum albumin immunogen with AuNP at an optimum pH and concentration followed by centrifugation |
| 36 | Colloidal AuNPs produced by laser ablation | 24 nm | UV-vis spectra and TEM | Detection: monoclonal antibodies anti-ZEA antibodies Capture: ZEA-BSA conjugate | Mixing of anti-ZEA antibodies with AuNP in an optimum pH and concentration followed by centrifugation |
| 37 | Gold nanorods | NA | DLS, zeta potential, Raman spectrum | Detection: monoclonal hepatitis B surface antibody (HBsAb) Capture: monoclonal hepatitis B surface antibody (HBsAb) | Mixing of monoclonal hepatitis B surface antibody (HBsAb) with AuNP in an optimum pH and concentration followed by centrifugation |
| 38 | Colloidal AuNPs | 40 nm | UV-vis spectra | Detection: monoclonal antibodies (mAb) 4C12 Capture: monoclonal antibodies (mAb) 3A9 | Mixing of mAb 4C12 with AuNP in an optimum pH and concentration followed by centrifugation |
| 39 | Colloidal AuNPs | 20 nm | UV-vis spectra | Detection: hemagglutinin protein H9AIV Capture: H9AIV hemagglutinin | Mixing of hemagglutinin protein H9AIV with AuNP in an optimum pH and concentration followed by centrifugation |
| 40 | Flowerlike AuNPs | 20 and 40 nm | UV-vis spectra, SEM, and TEM | Detection: murine anti-*E. coli* O157:H7 mAb) Capture: goat anti-*E.coli* O157:H7 pAb | Mixing of anti-*E. coli* O157:H7 mAb with AuNP in an optimum pH and concentration followed by centrifugation |
| 41 | Colloidal AuNPs | 20 nm, 60 nm, 100 nm, 180 nm | UV-vis spectroscopy, DLS and TEM | Detection: monoclonal antibodies anti-ochratoxin A Capture: biotin-labeled OTA–BSA conjugates | Mixing of Monoclonal antibodies anti-ochratoxin A with AuNP in an optimum pH and concentration followed by centrifugation |
| 42 | AuNPs produced by laser ablation | 20 nm | UV-vis spectroscopy and DLS | DNA | The "ex situ," i.e., mixing of DNA in a specific concentration to the laser-produced AuNPs |
| 43 | Gold nanoparticles (GNPs) | 20 nm | UV-vis spectroscopy and TEM | Detection: antibodies (anti-Tf antibody) Capture: secondary antibodies (anti-Tf antibody) | Mixing of the anti-Tf antibody with AuNP in an optimum pH and concentration followed by centrifugation. |
| 44 | Colloidal AuNPs | 15 nm | UV-vis spectroscopy and TEM | Detection: anti-CA15-3-HRP Capture: anti-CA15-3 | Mixing of anti-CA15-3-HRP with AuNP at an optimum pH and concentration followed by centrifugation |
| 45 | AuNPs (purchased) | 20 and 40 nm | DLS | Detection: antibodies to prostate-specific antigen Capture: monoclonal HS-5 anti-PSA | Mixing of antibodies to prostate-specific antigen with AuNP at an optimum pH and concentration followed by centrifugation |
| 46 | AuNPs | 13 nm | UV-vis spectroscopy | Detection: reporter DNA Capture: capture probe DNA conjugated with biotin | Mixing of thiolated DNA with synthesized gold nanoparticles in a specific concentration in the presence of salt |

**Table 1** (continued)

| | | | | | |
|---|---|---|---|---|---|
| 47 | AuNPs | 30–32 nm | DLS and TEM | Detection: mouse monoclonal antibodies against procalcitonin (IgG1 and IgG2) Capture: GNP–biotin conjugates | Mixing of mouse monoclonal antibodies against procalcitonin with AuNP in an optimum pH and concentration followed by centrifugation |
| 48 | AuNPs | 35 nm | UV-vis spectroscopy, DLS, and TEM | Detection: human IgG Capture: anti-human IgG | Mixing of Human IgG with AuNP in an optimum pH and concentration followed by centrifugation |
| 49 | Colloidal AuNPs | 40 nm | NA | Detection: anti-PA (Anthrax antibody) Capture: PA (Anthrax antigen) | Mixing of Anthrax antigen with AuNP in an optimum pH and concentration followed by centrifugation |
| 50 | Colloidal AuNPs | 15 nm | UV-vis spectroscopy, zeta potential, and TEM | Detection: monoclonal antibodies (mAbs) and barcode DNA Capture: Capture DNA | Mixing of monoclonal antibodies with AuNP and also mixing and incubating DNA along with NaCl in an optimum pH and concentration followed by centrifugation |
| 51 | Colloidal AuNPs (purchased) | 40 nm | NA | Detection: anti-HSV-2 IgG Capture: recombinant gG-1 antigen, purified native gG-2 antigen, and goat anti-human IgG antibody | Mixing of goat anti-human IgG with AuNP in an optimum pH and concentration followed by centrifugation |
| 52 | Colloidal AuNPs (purchased) | 20 nm | NA | Detection: rat monoclonal antibody (MAb) – Mab-JF5 Capture: Mab-JF5 | Mixing of monoclonal antibody (MAb) against galactomannan (GM)with AuNP at an optimum pH and concentration followed by centrifugation |
| 53 | AuNPs | 30 nm | NA | Detection: anti-protein A and anti-CRP antibodies Capture: anti-protein A and anti-CRP antibodies | Mixing of anti-protein A and anti-CRP antibodies with AuNP in an optimum pH and concentration followed by centrifugation |
| 54 | Colloidal AuNPs (purchased) | NA | NA | Detection: HA-tagged-IA-2 Capture: anti-HA-Tag antibody | Mixing of HA-tagged-IA-2 with AuNP at an optimum pH and concentration followed by centrifugation |
| 55 | Colloidal AuNPs, nanogold-polyaniline--nanogold microspheres (GPGs) and colloidal carbon | 40 nm | UV-vis spectra and TEM | Detection: anti-salbutamol antibodies(SAL) Capture: SAL-OVA antigen | Mixing of anti-salbutamol antibodies (SAL) with AuNP in an optimum pH and concentration followed by centrifugation |

| Sr. no. | Size of conjugated AuNPs | Characterization technique for conjugated AuNPs | Application | Reference |
|---|---|---|---|---|
| 1 | NA | NA | Detection of human cytomegalovirus | [58] |
| 2 | NA | NA | Detection of goose parvovirus | [94] |
| 3 | Size increased to about + 4 nm | UV-vis spectroscopy, DLS, TEM, FTIR, and EDS | The influence of nanoparticle size on conjugation and strip efficiency | [42] |
| 4 | NA | UV-vis spectroscopy | Detection of *Riemerella anatipestifer* | [18] |
| 5 | 53.13 nm after conjugation with DNA | DLS, Raman spectroscopy and SEM analysis | Detection of HIV-1 DNA | [95] |
| 6 | NA | UV-vis spectroscopy | Detection of human tetanus antibody in whole blood | [59] |
| 7 | NA | UV-vis spectroscopy and SPR | Analysis of conjugation properties on 10 nm AuNPs | [19] |
| 8 | NA | UV-vis spectroscopy and DLS | Detection of T-2 toxin | [81] |
| 9 | NA | UV-vis spectroscopy | Detection of snake venom | [96] |
| 10 | NA | UV-vis spectroscopy | Detection of mycotoxin | [97] |
| 11 | NA | UV-vis spectroscopy, TEM, and DLS | Detection of trypanosomiasis | [98] |
| 12 | | DLS and zeta analyzer. | The efficiency of different sizes of gold NPs for bioconjugation | [20] |

**Table 1** (continued)

| | | | | |
|---|---|---|---|---|
| | Size increased by 7 nm after protein conjugation | | | |
| 13 | NA | UV-vis spectroscopy and TEM | Detection of olaquindox | [77] |
| 14 | NA | UV-vis spectroscopy | Detection of Japanese encephalitis | [99] |
| 15 | NA | UV-vis, SPR, and TEM | Detection of fibrinogen and thrombin (not based on LFIS) | [80] |
| 16 | NA | UV-vis spectra and TEM | Enhancement of signal using AuNPs for detection of pathogens | [86] |
| 17 | NA | UV-vis spectra | Detection of Troponin 1 using dual gold nanoparticle conjugation | [100] |
| 18 | NA | NA | Detection of human interferon gamma | [28] |
| 19 | NA | DLS, UV-vis spectra, and fluorescence spectroscopy | Detection of microbial transglutaminase | [73] |
| 20 | NA | UV-vis spectra | Ultrasensitive biosensor for nucleic acid detection | [55] |
| 21 | NA | UV-vis spectra and TEM | Detection of *Toxoplasma gondii* infection in dogs and cats | [78] |
| 22 | NA | UV-vis spectra and TEM | Detection of Avian influenza and Newcastle disease viruses | [101] |
| 23 | NA | UV-vis spectra and TEM | Detection of antibodies to *Treponema pallidum* | [60] |
| 24 | NA | UV-vis spectra and TEM | Detection of chromium ions in water and serum samples | [102] |
| 25 | NA | UV-vis spectra, DLS and TEM | Detection of brugian filariasis | [21] |
| 26 | NA | UV-vis spectra and TEM | Microchip-based visual detection of interleukin-6 and tumor necrosis factor α | [103] |
| 27 | NA | UV-vis spectra, TEM and SPR | Detection of Tuberculosis | [104] |
| 28 | NA | TEM | Detection of *Mycoplasma suis* | [105] |
| 29 | NA | DLS, SPR, AFM, HR-TEM | Detection of Cortisol | [68] |
| 30 | NA | UV-vis spectroscopy, DLS, and TEM | Detection of *Staphylococcus aureus* | [74] |
| 31 | NA | UV-vis spectroscopy | Screening of microalbuminuria | [75] |
| 32 | NA | UV-vis spectra and TEM | Enhanced LFIS using AuNPs loaded with enzymes | [106] |
| 33 | NA | UV-vis spectra and TEM | Detection of *Salmonella typhi* in human serum | [107] |
| 34 | NA | UV-vis spectroscopy, DLS, and TEM | Polymer-modified AuNPs via RAFT polymerization | [57] |
| 35 | NA | UV-vis spectroscopy, HR-TEM, and AFM | Competitive immunochromatographic strip assay for 17-α-hydroxyprogesterone using colloidal AuNPs | [44] |
| 36 | NA | UV-vis spectra and TEM | Detection of zearalenone mycotoxin | [108] |
| 37 | NA | DLS, zeta potential, Raman spectrum | Detection of hepatitis B virus in the buffer, blood serum, and plasma | [109] |
| 38 | NA | UV-vis spectra | Rapid detection of *Streptococcus agalactiae* in tilapia | [110] |
| 39 | NA | UV-vis spectra | Quantitative detection of H9AIV antibodies | [111] |
| 40 | NA | UV-vis spectra, SEM, and TEM | Detection of *Escherichia coli* O157:H7 | [47] |
| 41 | NA | UV-vis spectroscopy, DLS, and TEM | Effect of different sized spherical AuNPs grown layer by layer on the sensitivity of LFIS | [112] |
| 42 | 38 nm and 72 nm produced by two different methods of conjugation | DLS | Characterization of laser-produced gold nanoparticle with dynamic light scattering | [33] |
| 43 | NA | Aqueous two-phase system (ATPS) partitioning of radiolabeled GNPs | An aqueous two-phase system for extraction of proteins from the interface for detection using a lateral flow immunoassay | [56] |
| 44 | NA | UV-vis spectroscopy | Detection of breast cancer biomarker (CA15-3 antigen) | [113] |
| 45 | 85 and 43 m | DLS | Increased sensitivity of LFIS using silver and gold enhancements | [114] |

**Table 1** (continued)

| | | | | |
|---|---|---|---|---|
| 46 | NA | UV-vis spectroscopy | Detection of DNA | [87] |
| 47 | NA | DLS and TEM | Detection of procalcitonin | [49] |
| 48 | 60 nm as observed by TEM | UV-vis spectroscopy, DLS, and TEM | Signal enhancement for nanoprobe-based biosensing | [115] |
| 49 | NA | NA | Detection of anti-anthrax antigen IgG in serum and whole blood | [116] |
| 50 | NA | UV-vis spectroscopy, zeta potential, and TEM | Detection of small molecules such as triazophos | [117] |
| 51 | NA | NA | Detection of herpes simplex virus type 2 antibodies in serum and whole blood | [118] |
| 52 | NA | NA | Detection of invasive aspergillosis in serum | [119] |
| 53 | NA | SEM analysis of the sample pad | Detection of protein A and C-reactive protein | [120] |
| 54 | NA | NA | Detection of tyrosine phosphatase-like protein IA-2 autoantibodies | [121] |
| 55 | NA | UV-vis spectra and TEM | Detection of salbutamol | [122] |

conjugating horseradish peroxidase (HRP) with AuNP, creating a double marker system for the detection of nucleic acids [55, 87]. The functionalization and conjugation of biomolecules with AuNPs are possible because gold has high compatibility with biological molecules compared to other metal nanoparticles used for biosensing. Thus, due to the optical properties, relative ease of synthesis, and flexibility in surface modification for functionalization and conjugation, AuNPs are mostly preferred for lateral flow biosensing devices.

## Disadvantages of using AuNPs in LFIS

Despite having numerous advantages, there are certain parameters to be considered before the utilization of colloidal AuNPs in LFIS. The major limitation exhibited by the AuNPs, for application in LFIS, is the low optical signal and low sensitivity. The recent developments in LFIS have focused on increasing the sensitivity and signal amplification strategies to overcome the challenges shown by AuNPs [88]. The signal amplification of gold nanoparticles is usually carried out using various size/shape of AuNPs, coupled with biorecognition steps such as DNA/RNA hybridization or protein-protein interaction. Also, dual sandwich ELISA using AuNP tags for both detection and the target antigen is a prominent technique used for signal amplification. For example, Si et al. [89] tagged the AuNPs with detection antibody, and the capture antibody was conjugated with biotin. The presence of a target antigen in the sample would form a bridge between the biotinylated capture antibody and AuNP-tagged detection antibody forming a dendritic nanoparticle complex. The signal intensity has been maximized due to the formation of the complex. For increasing the sensitivity, multiplex assays have been developed using gold nanoparticles. The signal generated by AuNPs is colorimetric and does not require a handheld reader, i.e., the result can be observed with naked eyes. Thus, the interpretation is qualitative, which can either give a positive or negative test result [90]. This limitation of using colloidal gold as the marker has been overcome by using other materials such as quantum dots, carbon dots, latex beads, and magnetic nanoparticles, which not only increases the sensitivity but also can be used for quantitative interpretation.

## Application of gold nanoparticles in immunosensing

Owing to the advantages, colloidal AuNPs have found its place among the most common and preferred nanomaterial used in the field of biosensors and diagnostics. Numerous biosensing applications have been developed using colloidal AuNPs. Biomedical applications such as cancer imaging and detection employ AuNPs in major proportion. Recently, AuNPs with surface-enhanced Raman scattering were used for in vivo cancer imaging in mice where 60 nm AuNP core was encapsulated with 15-nm-thick silica shell where the

**Table 2** Application of gold nanoparticles-based LFIS in food safety

| Sr. no. | Type of gold nanoparticle (AuNP) | Size of AuNPs | Characterization techniques for AuNPs | Type of conjugation material | Technique used for conjugation |
|---|---|---|---|---|---|
| 1 | Colloidal AuNPs | 17 nm | UV-vis spectroscopy and TEM | Detection: rabbit anti-human IgG Capture: excretory-secretory antigen of *Paragonimus skrjabini* | Mixing of rabbit anti-human IgG with AuNP in an optimum pH and concentration followed by centrifugation. The pellet was suspended in PBS containing BSA |
| 2 | Spherical AuNPs; Au-Ag hollow nanoparticle | 18 nm | UV-vis spectroscopy, SEM, and TEM | Detection: anti-CLE antibody Capture: CLE antigen | Mixing of the anti-CLE antibody with AuNP in an optimum pH and concentration followed by centrifugation |
| 3 | Colloidal AuNPs | 15 nm | UV-vis spectroscopy | Detection: monoclonal antibody against sulfamonomethoxine (anti-SMM) Capture: SMM antigen | Mixing of anti-SMM with AuNP in an optimum pH and concentration followed by centrifugation |
| 4 | Colloidal AuNPs | 15 nm | UV-vis spectroscopy and TEM | Detection: mAb against papaverine Capture: PAPA-ovalbumin antigen | Mixing of anti-PAPA with AuNP in an optimum pH and concentration followed by centrifugation |
| 5 | Colloidal AuNPs | 34 nm | TEM | Detection: Both purified antibody and native antiserum (anti-ofloxacin) Capture: ofloxacin–protein | Mixing of anti-ofloxacin with AuNP in an optimum pH and concentration followed by centrifugation |
| 6 | Colloidal AuNPs and Anodic Stripping Voltammetry (ASV) of gold. | 17 nm | UV-vis spectra and FT-IR spectroscopy and TEM | Detection: anti-melamine (AuNP-antimel) Capture: anti-melamine (AuNP-antimel) | Mixing of AuNP-antimel with AuNP in an optimum pH and concentration followed by centrifugation |
| 7 | Colloidal AuNPs, nanogold-polyaniline--nanogold microspheres (GPGs) and colloidal carbon | 40 nm | UV-vis spectra and TEM | Detection: anti-salbutamol antibodies(SAL) Capture: SAL-OVA antigen | Mixing of Anti-salbutamol antibodies (SAL) with AuNP in an optimum pH and concentration followed by centrifugation |
| 8 | Desert rose-like gold nanoparticles (DR-GNPs) | 72 nm | UV-vis spectroscopy, DLS, and TEM | Detection: polyclonal antibodies against aflatoxin B1 (AFB1) and fumonisins (FMs) Capture: polyclonal antibodies against aflatoxin B1 (AFB1) and fumonisins (FMs) | Mixing of polyclonal antibodies against aflatoxin B1 (AFB1) and fumonisins (FMs) with AuNP in an optimum pH and concentration followed by centrifugation |
| 9 | Colloidal AuNPs | 10 nm | UV-vis spectra | Detection: monoclonal antibodies MAb VC-273 Capture: MAb VC-812 | Mixing of MAb VC-273 with AuNP in an optimum pH and concentration followed by centrifugation |
| 10 | Colloidal AuNPs | 25 nm | TEM | Detection: polyclonal antibody (Pab) against staphylococcal enterotoxin B (SEB) Capture: polyclonal antibody (Pab) against staphylococcal enterotoxin B (SEB) | Mixing of Pab against staphylococcal with AuNP in an optimum pH and concentration followed by centrifugation |
| 11 | Colloidal AuNPs | 20 nm | TEM | Detection: monoclonal antibodies against fumonisins Capture: monoclonal antibodies against fumonisins | Mixing of monoclonal antibodies against fumonisins with AuNP in an optimum pH and concentration followed by centrifugation |
| 12 | Colloidal AuNPs | NA | NA | Detection: monoclonal antibodies anti-AFB1 antibodies Capture: AFB1-BSA conjugate | Mixing of anti-AFB1 with AuNP in an optimum pH and concentration followed by centrifugation |
| 13 | Colloidal AuNPs | 15 nm | UV-vis spectra and TEM | Detection: Monoclonal antibodies against 3-amino-2-oxazolidinone (AOZ), semicarbazide (SEM), 3-amino-5-methylmorpholino-2-oxazolidinone (AMOZ), and 1-aminohydantoin (AHD) Capture: antigens of 3-amino-2-oxazolidinone (AOZ), semicarbazide (SEM), 3-amino-5-methylmorpholino-2-oxazolidinone | Mixing of array antibodies with AuNP in an optimum pH and concentration followed by centrifugation |

**Table 2** (continued)

| | | | | | |
|---|---|---|---|---|---|
| | | | | (AMOZ), and 1-aminohydantoin (AHD) | |
| 14 | Colloidal AuNPs | NA | NA | Detection: monoclonal antibodies (mAbs) against estrone (E1), 17β-estradiol (17β-E2), and estriol (E3) Capture: haptens of E1, 17β-E2, and E3 | Mixing of mAbs against estrone (E1), 17β-estradiol (17β-E2), and estriol (E3) with AuNP at an optimum pH and concentration followed by centrifugation |
| 15 | Colloidal AuNPs | 20 nm | UV-vis spectra and TEM | Detection: monoclonal antibodies against okadaic acid Capture: monoclonal antibodies against okadaic acid | Mixing of Monoclonal antibodies against okadaic acid with AuNP at an optimum pH and concentration followed by centrifugation |
| 16 | Colloidal AuNPs | 20 nm | UV-vis spectra and TEM | Detection: group-specific monoclonal antibody (mAb) Capture: hapten 1 with a thiazole ring, hapten 2 with a benzene ring, and hapten 3 with a straight carbon chain | Mixing of a group-specific monoclonal antibody with AuNP in an optimum pH and concentration followed by centrifugation |
| 17 | Colloidal AuNPs | 40 nm | UV-vis spectroscopy, DLS, and TEM | Detection: monoclonal antibodies against bisphenol A Capture: BPA-BSA conjugates | Mixing of monoclonal antibodies against bisphenol A with AuNP in an optimum pH and concentration followed by centrifugation |
| 18 | Spherical AuNP | 15 nm | NA | Detection: monoclonal antibodies against staphylococcal enterotoxin A, B, C, D, and E Capture: monoclonal antibodies against staphylococcal enterotoxin A, B, C, D, and E | Mixing of Monoclonal antibodies against staphylococcal enterotoxin A, B, C, D, and E with AuNP in an optimum pH and concentration followed by centrifugation |
| 19 | AuNPs (purchased) | 40 nm | Flocculation assay | Detection: monoclonal antibodies Anti-O1 LPS mAb and anti-O139 LPS mAb Capture:monoclonal antibodies Anti-O1 LPS mAb and anti-O139 LPS mAb | Mixing of Anti-O1 LPS mAb and anti-O139 LPS mAb with AuNP at an optimum pH and concentration followed by centrifugation |
| 20 | Colloidal AuNPs | 40 nm | UV-vis spectra and TEM | Detection: polyclonal antibodies (pAb) specific to fumonisinB1 Capture: fumonisinB1–OVA | Mixing of polyclonal antibodies (pAb) specific to fumonisinB1 with AuNP in an optimum pH and concentration followed by centrifugation |
| 21 | Colloidal AuNPs | 40 nm | UV-vis spectra and TEM | Detection: polyclonal antibody(PAb) raised against FB1 Capture: FB1-OVA conjugate | Mixing of polyclonal antibody(PAb) raised against FB1with AuNP at an optimum pH and concentration followed by centrifugation |
| 22 | Urchin-like gold nanoparticle (UGN) | 60 nm | UV-vis spectra and TEM | Detection: monoclonal antibodies against FB1–carbodiimide (EDCA)–KLH Capture: BSA–FB1 conjugate | Mixing of monoclonal antibodies against FB1–carbodiimide (EDCA)–KLH with AuNP in an optimum pH and concentration followed by centrifugation |
| 23 | Colloidal AuNPs | 40 nm | UV-vis spectra and TEM | Detection: polyclonal antibody against FB1 Capture: BSA-fumonisin conjugate | Mixing of polyclonal antibody against FB1 with AuNP at an optimum pH and concentration followed by centrifugation |
| 24 | Colloidal AuNPs | 40 nm | UV-vis spectra and TEM | Detection: polyclonal antibodies against ochratoxin A(OTA) Capture: OTA-BSA conjugate | Mixing of polyclonal antibodies against ochratoxin A(OTA) with AuNP at an optimum pH and concentration followed by centrifugation |
| 25 | Colloidal AuNPs | 40 nm | UV-vis spectra and TEM | Detection: polyclonal antibodies against aflatoxin M1 Capture: aflatoxin M1-BSA conjugate | Mixing of polyclonal antibodies against aflatoxin M1 with AuNP at an optimum pH and concentration followed by centrifugation |
| 26 | Colloidal AuNPs | 20 nm | UV-vis spectra, DLS and SEM | Detection: polyclonal antibodies against oxytetracycline (OTC) Capture: OTC-BSA conjugate | Mixing of polyclonal antibodies against oxytetracycline (OTC) with AuNP at an optimum pH and concentration followed by centrifugation |
| 27 | Colloidal AuNPs | 15–60 nm | UV-vis spectroscopy and TEM | Detection: monoclonal anti-mycotoxin antibodies Capture: | Mixing of monoclonal anti-mycotoxin antibodies with AuNP in an optimum pH and concentration followed by centrifugation (15 and 40 nm sizes were selected for conjugation with antibodies) |

| Sr. no. | Size of conjugated AuNPs | Characterization technique for conjugated AuNPs | Application | Reference |
|---|---|---|---|---|
| 1 | 18–20 nm | UV-vis spectroscopy and TEM | Detection of paragonimiasis | [46] |

**Table 2** (continued)

| | | | | |
|---|---|---|---|---|
| 2 | NA | NA | Detection of clenbuterol | [52] |
| 3 | NA | UV-vis spectroscopy | Detection of sulfamonomethoxine | [123] |
| 4 | NA | UV-Vis spectroscopy | Detection of papaverine in pure ginger powder | [76] |
| 5 | NA | TEM | Detection of ofloxacin in food | [124] |
| 6 | NA | UV-vis spectra and FT-IR spectroscopy and TEM | ASV of gold at boron-doped diamond electrode for detection of melamine | [67] |
| 7 | NA | UV-vis spectra and TEM | Detection of salbutamol | [122] |
| 8 | NA | UV-vis spectroscopy, DLS, and TEM | Determination of aflatoxinB1 and fumonisin | [125] |
| 9 | NA | UV-vis spectra | Detection of *Vibrio cholerae* O139 in seafood samples | [126] |
| 10 | NA | TEM | Detection of *Staphylococcal enterotoxin B* | [127] |
| 11 | NA | TEM | Rapid screening of fumonisins B1, B2, and B3 in maize | [128] |
| 12 | NA | NA | Detection of aflatoxin B1 | [129] |
| 13 | NA | UV-vis spectra and TEM | Detection of four nitrofuran metabolites in fish samples | [53] |
| 14 | NA | NA | Detection of three natural estrogens in milk | [130] |
| 15 | NA | UV-vis spectra and TEM | On-site detection of okadaic acid in shellfish products | [131] |
| 16 | NA | UV-vis spectra and TEM | Rapid detection of twenty-six sulfonamides in foods | [132] |
| 17 | NA | UV-vis spectroscopy, DLS, and TEM | On-site detection of bisphenol A | [17] |
| 18 | NA | NA | Multiplexed LFIS for simultaneous detection of staphylococcal enterotoxin A, B, C, D, and E | [54] |
| 19 | NA | Flocculation assay | Detection of *Vibrio cholerae* serogroups O1 and O139 | [133] |
| 20 | NA | UV-vis spectra and TEM | Detection of fumonisin B1 in grain-based food and feed samples | [134] |
| 21 | NA | UV-vis spectra and TEM | Detection of fumonisin B1 from cereal samples | [135] |
| 22 | NA | UV-vis spectra and TEM | Detection of fumonisin B1 in grains | [136] |
| 23 | NA | UV-vis spectra and TEM | Detection of fumonisins in maize | [15] |
| 24 | NA | UV-vis spectra and TEM | Detection of ochratoxin A | [137] |
| 25 | NA | UV-vis spectra and TEM | Detection of aflatoxin M1 in milk | [138] |
| 26 | NA | UV-vis spectra, DLS and SEM | Detection of oxytetracycline residues in milk | [139] |
| 27 | NA | UV-vis spectroscopy and TEM | Detection of anti-mycotoxin antibodies (e.g., zearalenone) | [79] |

**Table 3** Application of gold nanoparticles-based LFIS in environmental monitoring

| Sr. no. | Type of gold nanoparticle (AuNP) | Size of AuNPs | Characterization techniques for AuNPs | Type of conjugation material | Technique used for conjugation | Size of conjugated AuNPs | Characterization technique for conjugated AuNPs | Application | Reference |
|---|---|---|---|---|---|---|---|---|---|
| 1 | Colloidal AuNPs | 40 nm | UV-vis spectra and TEM | Detection: anti-chlorpyrifos-methyl mAb<br>Capture: hapten-BSA(H1-BSA) | Mixing of anti-chlorpyrifos-methyl mAb with AuNP in an optimum pH and concentration followed by centrifugation | NA | UV-vis spectra and TEM | Detection of chlorpyrifos-methyl in water samples | [140] |
| 2 | Colloidal AuNPs | 40 nm | UV-vis spectra and TEM | Detection: anti-chlorpyrifos antibody<br>Capture: hapten–OVA (ovalbumin) conjugate | Mixing of the anti-chlorpyrifos antibody with AuNP in an optimum pH and concentration followed by centrifugation | NA | UV-vis spectra and TEM | Detection of the organophosphorus pesticide chlorpyrifos | [141] |
| 3 | Colloidal AuNPs | 20 nm | UV-vis spectra and TEM | Detection: monoclonal antibodies anti-Cr-EDTA McAb<br>Capture: antigen Cr-EDTA-BSA | Mixing of anti-Cr-EDTA with AuNP in an optimum pH and concentration followed by centrifugation | NA | UV-vis spectra and TEM | Detection of chromium ions in water and serum samples | [102] |
| 4 | Colloidal AuNPs | 40 nm | NA | Detection: monoclonal antibodies (anti-imidacloprid, anti-chlorpyrifos-methyl and anti-isocarbophos mAbs)<br>Capture: Antigens for the same compounds | Mixing of anti-imidacloprid, anti-chlorpyrifos-methyl and anti-isocarbophos mAbs with AuNP at an optimum pH and concentration followed by centrifugation | NA | UV-vis spectroscopy | A bare-eye-based LFIS for simultaneous detection of three pesticides | [142] |
| 5 | Colloidal AuNPs | 20 nm | UV-vis spectra and TEM | Detection: monoclonal antibodies-gold quencher mAb-gold quencher<br>Capture: BSA-labeled FNPs | Mixing of Monoclonal antibodies-gold quencher mAb-gold quencher with AuNP at an optimum pH and concentration followed by centrifugation | NA | UV-vis spectra and TEM | Fluorescence-quenching LFIS for detection of the heavy metal chromium | [143] |

Raman reporter was embedded [91]. As with the case of immunosensing, paper-based methods are most widely because of their ease of handling. But it also presents drawbacks such as low colorimetric signal. Recently a strategy was developed to tackle this drawback. Cellulose nanofibers were embedded inside the paper, which would concentrate the amount of capture antibody on the surface and hence will increase the signal in the test line when bound with AuNPs [92]. Figure 5 shows the incorporation of cellulose nanofibers into the paper and how it has helped to increase the signal in the test line. Another recent work focuses on label-free detection of foodborne pathogens with the use of positively charged AuNPs, which combines with a negatively charged bacterial cell wall, and then this complex is captured on the test line with proper antibodies [93]. Figure 6 shows the schematic illustration of the label-free approach for detection of foodborne pathogens.

Tables 1, 2, and 3 describe the LFIS applications involving AuNPs with emphasis on the type of conjugation material, techniques used for the bioconjugation, and characterization of nanoparticles and conjugated nanoparticles. The tables enlist LFIS techniques developed utilizing gold nanoparticles for application in human and animal healthcare, food safety, and environmental monitoring.

## Summary and future perspective

Gold nanoparticles have been used since long for the development of paper-based biosensing platforms such as LFIS. Due to its exceptional physical and chemical properties, its characterization by application in biosensing has been of prime interest among researchers. From the literature, it is evident that the chemical method for the synthesis of AuNPs is most commonly used. The proper analysis must be carried out using different characterization techniques for a better understanding of the AuNPs that have been used for the application. Conjugation of a biomolecule with AuNPs is obligatory to utilize in biosensing applications. Tables 1, 2, and 3 present the application of colloidal AuNPs for the development of biosensors and LFIS having utility in various areas. The emphasis was on various characterization techniques reported in the literature to analyze the size, shape, and polydispersity of AuNPs as well as bioconjugated AuNPs. It is found that although some reports have mentioned the details of characterization such as the size and shape of nanoparticle synthesized, its polydispersity, the difference in size when conjugated with protein, etc., data representation is insufficient for the characterization of bioconjugated AuNPs. To demonstrate the successful conjugation of AuNPs with the biological molecules, an array of techniques such as FTIR, AFM, HR-TEM, EDS, and SDS PAGE along with the conventional techniques of UV-vis spectroscopy, DLS, and TEM should be used. The future studies for the development of LFIS should have detailed information on the characterization techniques for both nanoparticle synthesis and its bioconjugation.

**Funding information** Dr. Vivek Borse would like to acknowledge the Department of Science and Technology Ministry of Science and Technology, Government of India for the INSPIRE Faculty Award (IFA18-ENG266, DST/INSPIRE/04/2018/000991). RDJ would like to acknowledge the financial support from The Campbell Foundation (Florida, USA) and start-up funds from the Department of Pharmaceutical Sciences, JH School of Pharmacy, Texas Tech University Health Sciences Center (TTUHSC), TX, USA. PP is thankful to the Indian Council of Medical Research, India for Research Funding (No.5/4–5/159/Neuro/2015-NCD-I) and H. R. Patel Institute of Pharmaceutical Education and Research, Shirpur for providing necessary facilities.

## Compliance with ethical standards

**Conflict of interests** The authors declare that they have no conflicts of interest.

## References

1. Bagchi S, Chhibber T, Lahooti B, Verma A, Borse V, Jayant RD. In-vitro blood-brain barrier models for drug screening and permeation studies: an overview. *Drug Des Devel Ther*. 2019;13:3591–605.
2. Pawar V, Borse V, Thakkar R, Srivastava R. Dual-purpose injectable doxorubicin conjugated alginate gel containing polycaprolactone microparticles for anti-cancer and anti-inflammatory therapy. Curr Drug Deliv. May 2018;15(5):716–26.
3. Patil PO, Pandey GR, Patil AG, Borse VB, Deshmukh PK, Patil DR, et al. Graphene-based nanocomposites for sensitivity enhancement of surface plasmon resonance sensor for biological and chemical sensing: a review. Biosens Bioelectron. Aug. 2019;139:111324.
4. Borse V, Thakur M, Sengupta S, Srivastava R. N-doped multifluorescent carbon dots for 'turn off-on' silver-biothiol dual sensing and mammalian cell imaging application. Sensors Actuators B Chem. Sep. 2017;248:481–92.
5. Borse V, Kashikar A, Srivastava R. Fluorescence stability of Mercaptopropionic acid capped cadmium telluride quantum dots in various biochemical buffers. J Nanosci Nanotechnol. 2018;18(4):2582–91.
6. V. Borse, M. Sadawana, and R. Srivastava, "CdTe quantum dots: aqueous phase synthesis, stability studies and protein conjugation for development of biosensors," in *SPIE Photonics* Europe, 2016, p. 988423.
7. Borse V, Jain P, Sadawana M, Srivastava R. 'Turn-on' fluorescence assay for inorganic phosphate sensing. Sensors Actuators B Chem. Mar. 2016;225:340–7.
8. Borse V, Pawar V, Shetty G, Mullaji A, Srivastava R. Nanobiotechnology perspectives on prevention and treatment of orthopaedic implant associated infection. Curr Drug Deliv. 2016;13(2):175–85.
9. Borse V, Kaler A, Banerjee UC. Microbial synthesis of platinum nanoparticles and evaluation of their anticancer activity. Int J Emerg Trends Electr Electron. 2015;11(2):2320–9569.
10. Khandelia R, Bhandari S, Pan UN, Ghosh SS, Chattopadhyay A. Gold nanocluster embedded albumin nanoparticles for two-

photon imaging of Cancer cells accompanying drug delivery. Small. Sep. 2015;11(33):4075–81.
11. Sahoo AK, Banerjee S, Ghosh SS, Chattopadhyay A. Simultaneous RGB emitting au nanoclusters in chitosan nanoparticles for anticancer gene theranostics. ACS Appl Mater Interfaces. Jan. 2014;6(1):712–24.
12. Kaushik A, et al. A sensitive electrochemical immunosensor for label-free detection of Zika-virus protein. *Sci Rep*. 2018;8(1): 9700.
13. Jayant RD, Atluri VS, Agudelo M, Sagar V, Kaushik A, Nair M. Sustained-release nanoART formulation for the treatment of neuroAIDS. Int J Nanomedicine. 2015;10:1077.
14. Banerjee M, Sharma S, Chattopadhyay A, Ghosh SS. Enhanced antibacterial activity of bimetallic gold-silver core-shell nanoparticles at low silver concentration. Nanoscale. Dec. 2011;3(12):5120–5.
15. Anfossi L, Calderara M, Baggiani C, Giovannoli C, Arletti E, Giraudi G. Development and application of a quantitative lateral flow immunoassay for fumonisins in maize. Anal Chim Acta. 2010;682(1–2):104–9.
16. Zhao Y, Zhang G, Liu Q, Teng M, Yang J, Wang J. Development of a lateral flow colloidal gold immunoassay strip for the rapid detection of enrofloxacin residues. J Agric Food Chem. Dec. 2008;56(24):12138–42.
17. Mei Z, Deng Y, Chu H, Xue F, Zhong Y, Wu J, et al. Immunochromatographic lateral flow strip for on-site detection of bisphenol a. Microchim Acta. Feb. 2013;180(3–4):279–85.
18. Hou W, et al. Development of colloidal gold immunochromatographic strips for detection of Riemerella anatipestifer. *PLoS One*. 2015;10(3):e0122952.
19. Siti RM, Khairunisak AR, Azlan AA, Noordin R. Green synthesis of 10 nm gold nanoparticles via seeded-growth method and its conjugation properties on lateral flow immunoassay. Adv Mater Res. 2013;686:8–12.
20. K. Rahme and J. D. Holmes, "Gold nanoparticles: synthesis, characterization, and bioconjugation," in *Dekker Encyclopedia of Nanoscience and Nanotechnology, Third Edition*, no. September, Taylor & Francis, 2015, pp. 1–11.
21. Makhsin SR, Razak KA, Noordin R, Zakaria ND, Chun TS. The effects of size and synthesis methods of gold nanoparticle-conjugated MαHIgG4 for use in an immunochromatographic strip test to detect brugian filariasis. *Nanotechnology*. 2012;23(49): 495719.
22. Nguyen ND, Dang VP, Le AQ, Nguyen QH. Electron beam/ $\gamma$ -ray irradiation synthesis of gold nanoparticles and investigation of antioxidant activity. *Adv Nat Sci Nanosci Nanotechnol*. 2014;5(4): 045002.
23. Zhou Y, Wang CY, Zhu YR, Chen ZY. A novel ultraviolet irradiation technique for shape-controlled synthesis of gold nanoparticles at room temperature. Chem Mater. Sep. 1999;11(9):2310–2.
24. Augustine AK, Nampoori VPN, Kailasnath M. Rapid synthesize of gold nanoparticles by microwave irradiation method and its application as an optical limiting material. Optik (Stuttg). 2014;125(22):6696–9.
25. Noruzi M, Zare D, Davoodi D. A rapid biosynthesis route for the preparation of gold nanoparticles by aqueous extract of cypress leaves at room temperature. Spectrochim Acta Part A Mol Biomol Spectrosc. Aug. 2012;94:84–8.
26. Narayanan KB, Sakthivel N. Phytosynthesis of gold nanoparticles using leaf extract of Coleus amboinicus Lour. Mater Charact. Nov. 2010;61(11):1232–8.
27. Mukherjee P, Senapati S, Mandal D, Ahmad A, Khan MI, Kumar R, et al. Extracellular synthesis of gold nanoparticles by the fungus Fusarium oxysporum. ChemBioChem. May 2002;3(5):461–3.
28. Chou SF. Development of a manual self-assembled colloidal gold nanoparticle- immunochromatographic strip for rapid determination of human interferon-γ. Analyst. 2013;138(9):2620–3.
29. Jazayeri MH, Amani H, Pourfatollah AA, Pazoki-Toroudi H, Sedighimoghaddam B. Various methods of gold nanoparticles (GNPs) conjugation to antibodies. Sens Bio-Sensing Res. Jul. 2016;9:17–22.
30. Arshi N, Ahmed F, Kumar S, Anwar MS, Lu J, Koo BH, et al. Microwave assisted synthesis of gold nanoparticles and their antibacterial activity against Escherichia coli (E. coli). Curr Appl Phys. 2011;11(1 SUPPL):S360–3.
31. Liu YC, Lin LH, Chiu WH. Size-controlled synthesis of gold nanoparticles from bulk gold substrates by sonoelectrochemical methods. J Phys Chem B. 2004;108(50):19237–40.
32. Sylvestre J, et al. Surface chemistry of gold nanoparticles produced by laser ablation in aqueous MediaSylvestre, J. et al., 2004. Surface chemistry of gold nanoparticles produced by laser ablation in aqueous media. The journal of physical chemistry B, 108(43), pp.16864–1686. J Phys Chem B. 2004;108(43):16864–9.
33. M. Zimbone *et al.*, "Dynamic light scattering on bioconjugated laser generated gold nanoparticles," *PLoS One*, vol. 9, no. 3, p. e89048, 2014.
34. Turkevich J, Stevenson PC, Hillier J. A study of the nucleation and growth processes in the synthesis of colloidal gold. Discuss Faraday Soc. 1951;11(c):55–75.
35. Frens G. Controlled nucleation for the regulation of the particle size in monodisperse gold suspensions. Nat Phys Sci. 1973;241(105):20–2.
36. Brown KR, Natan MJ. Hydroxylamine seeding of colloidal Au nanoparticles in solution and on surfaces. Langmuir. 1998;14(4): 726–8.
37. Kumari M, et al. Physico-chemical condition optimization during biosynthesis lead to development of improved and catalytically efficient gold nano particles. *Sci Rep*. 2016;6(1):27575.
38. Baek K, Patra JK. Novel green synthesis of gold nanoparticles using *Citrullus lanatus* rind and investigation of proteasome inhibitory activity, antibacterial, and antioxidant potential. *Int J Nanomedicine*. 2015;10(1):7253.
39. Ahmad A, Mukherjee P, Senapati S, Mandal D, Khan MI, Kumar R, et al. Extracellular biosynthesis of silver nanoparticles using the fungus Fusarium oxysporum. Colloids Surf B: Biointerfaces. 2003;28(4):313–8.
40. Das SK, Dickinson C, Lafir F, Brougham DF, Marsili E. Synthesis, characterization and catalytic activity of gold nanoparticles biosynthesized with Rhizopus oryzae protein extract. *Green Chem*. 2012;14(5):1322.
41. Zhang T, Wang W, Zhang D, Zhang X, Ma Y, Zhou Y, et al. Biotemplated synthesis of gold nanoparticle-bacteria cellulose nanofiber nanocomposites and their application in biosensing. Adv Funct Mater. Mar. 2010;20(7):1152–60.
42. Lou S, Ye J, Li K, Wu A. A gold nanoparticle-based immuno chromatographic assay: the influence of nanoparticulate size. Analyst. 2012;137(5):1174–81.
43. Singh M, Chandrasekaran N, Mukherjee A, Kumar M, Kumaraguru AK. Cancerous cell targeting and destruction using pH stabilized amperometric bioconjugated gold nanoparticles from marine macroalgae, Padina gymnospora. Bioprocess Biosyst Eng. Sep. 2014;37(9):1859–69.
44. Tripathi V, Nara S, Singh K, Singh H, Shrivastav TG. A competitive immunochromatographic strip assay for 17-α-hydroxy progesterone using colloidal gold nanoparticles. Clin Chim Acta. 2012;413(1–2):262–8.
45. Malarkodi C, Rajeshkumar S, Vanaja M, Paulkumar K, Gnanajobitha G, Annadurai G. Eco-friendly synthesis and

characterization of gold nanoparticles using *Klebsiella pneumoniae*. *J Nanostructure Chem*. 2013;3(1):30.
46. Wang Y, et al. Preparation of colloidal gold immunochromatographic strip for detection of Paragonimiasis skrjabini. *PLoS One*. 2014;9(3):e92034.
47. Zhang L, Huang Y, Wang J, Rong Y, Lai W, Zhang J, et al. Hierarchical flowerlike gold nanoparticles labeled immunochromatography test strip for highly sensitive detection of Escherichia coli O157:H7. Langmuir. 2015;31(19):5537–44.
48. Chandra P, Noh HB, Pallela R, Shim YB. Ultrasensitive detection of drug resistant cancer cells in biological matrixes using an amperometric nanobiosensor. Biosens Bioelectron. Aug. 2015;70:418–25.
49. Taranova NA, Urusov AE, Sadykhov EG, Zherdev AV, Dzantiev BB. Bifunctional gold nanoparticles as an agglomeration-enhancing tool for highly sensitive lateral flow tests: a case study with procalcitonin. Microchim Acta. Oct. 2017;184(10):4189–95.
50. Nikkhah-Moshaie R, Kaushik A, Jayant RD, Bhardwaj V, Nair M. TEM investigation of Nanocarriers distribution in mice brain. Microsc Microanal. Jul. 2016;22(S3):1172–3.
51. Zhu Y, Chandra P, Shim Y-B. Ultrasensitive and selective electrochemical diagnosis of breast cancer based on a hydrazine–au nanoparticle–aptamer bioconjugate. Anal Chem. Jan. 2013;85(2):1058–64.
52. J. Wang *et al.*, "Hollow Au-Ag nanoparticles labeled immunochromatography strip for highly sensitive detection of clenbuterol," *Sci. Rep.*, vol. 7, no. 1, p. 41419, 2017.
53. Wang Q, Liu Y, Wang M, Chen Y, Jiang W. A multiplex immunochromatographic test using gold nanoparticles for the rapid and simultaneous detection of four nitrofuran metabolites in fish samples. Anal Bioanal Chem. Jan. 2018;410(1):223–33.
54. Wang W, Liu L, Xu L, Kuang H, Zhu J, Xu C. Gold-nanoparticle-based multiplexed immunochromatographic strip for simultaneous detection of staphylococcal enterotoxin a, B, C, D, and E. Part Part Syst Charact. Jul. 2016;33(7):388–95.
55. He Y, Zhang S, Zhang X, Baloda M, Gurung AS, Xu H, et al. Ultrasensitive nucleic acid biosensor based on enzyme-gold nanoparticle dual label and lateral flow strip biosensor. Biosens Bioelectron. Jan. 2011;26(5):2018–24.
56. Chiu RYT, Thach AV, Wu CM, Wu BM, Kamei DT. An aqueous two-phase system for the concentration and extraction of proteins from the interface for detection using the lateral-flow immunoassay. *PLoS One*. 2015;10(11):e0142654.
57. Takara M, Toyoshima M, Seto H, Hoshino Y, Miura Y. Polymer-modified gold nanoparticles via RAFT polymerization: a detailed study for a biosensing application. Polym Chem. 2014;5(3):931–9.
58. Xiang L, Li L. Development and evaluation of an immunochromatographic strip for the detection of human cytomegalovirus. Lett Appl Microbiol. Mar. 2011;52(3):233–8.
59. Liu J, et al. A lateral flow assay for the determination of human tetanus antibody in whole blood by using gold nanoparticle labeled tetanus antigen. Microchim Acta. Feb. 2018;185(2):1–7.
60. Lin LR, Fu ZG, Dan B, Jing GJ, Tong ML, Chen DT, et al. Development of a colloidal gold-immunochromatography assay to detect immunoglobulin G antibodies to Treponema pallidum with TPN17 and TPN47. Diagn Microbiol Infect Dis. Nov. 2010;68(3):193–200.
61. Loo C, et al. Gold nanoshell bioconjugates for molecular imaging in living cells. *Opt Lett*. 2005;30(9):1012.
62. V. Singh, S. P. N. Nair, and G. K. Aradhyam, "Chemistry of conjugation to gold nanoparticles affects G-protein activity differently," *J. Nanobiotechnology*, vol. 11, no. 1, p. 7, 2013.
63. Schroedter A, Weller H. Ligand design and bioconjugation of colloidal gold nanoparticles. Angew Chem Int Ed. 2002;41(17):3218–21.
64. Rayavarapu RG, Petersen W, Ungureanu C, Post JN, van Leeuwen TG, Manohar S. Synthesis and bioconjugation of gold nanoparticles as potential molecular probes for light-based imaging techniques. Int J Biomed Imaging. 2007;2007:1–10.
65. Thobhani S, Attree S, Boyd R, Kumarswami N, Noble J, Szymanski M, et al. Bioconjugation and characterisation of gold colloid-labelled proteins. J Immunol Methods. 2010;356(1–2):60–9.
66. Zijlstra P, Paulo PMR, Yu K, Xu Q-H, Orrit M. Chemical interface damping in single gold nanorods and its near elimination by tip-specific functionalization. Angew Chem Int Ed. Aug. 2012;51(33):8352–5.
67. Ivandini TA, Wicaksono WP, Saepudin E, Rismetov B, Einaga Y. Anodic stripping voltammetry of gold nanoparticles at boron-doped diamond electrodes and its application in immunochromatographic strip tests. Talanta. Mar. 2015;134:136–43.
68. Nara S, Tripathi V, Singh H, Shrivastav TG. Colloidal gold probe based rapid immunochromatographic strip assay for cortisol. Anal Chim Acta. Dec. 2010;682(1–2):66–71.
69. Borse V, Srivastava R. Fluorescence lateral flow immunoassay based point-of-care nanodiagnostics for orthopedic implant-associated infection. *Sensors Actuators B Chem*. 2019;280(September 2017):24–33.
70. Borse V, Srivastava R. Process parameter optimization for lateral flow immunosensing. Mater Sci Energy Technol. 2019;2(3):434–41.
71. V. Borse, A. S. Patil, and R. Srivastava, "Development and testing of portable fluorescence reader (PorFloR™)," in *2017 9th International Conference on Communication Systems and Networks (COMSNETS)*, 2017, pp. 498–501.
72. Makkar RL, Syeda Aliya S, Borse V, Srivastava R. Design and development of portable fluorescence reader using silicon photo multiplier (SiPM) sensor. *Optical Sensing and Detection V*. 2018:106800B, 12.
73. Fan D, et al. Colloidal gold probe-based Immunochromatographic strip assay for the rapid detection of microbial transglutaminase in frozen Surimi. J Chemother. 2016;2016:1–7.
74. Niu K, Zheng X, Huang C, Xu K, Zhi Y, Shen H, et al. A colloidal gold nanoparticle-based immunochromatographic test strip for rapid and convenient detection of Staphylococcus Aureus. J Nanosci Nanotechnol. 2014;14(7):5151–6.
75. Omidfar K, Kia S, Larijani B. Development of a colloidal gold-based immunochromatographic test strip for screening of microalbuminuria. Hybridoma. 2011;30(2):117–24.
76. Ge W, Suryoprabowo S, Zheng Q, Kuang H. Development of an immunochromatographic test strip for the detection of papaverine in pure ginger powder. Food Agric Immunol. 2017;28(6):1304–14.
77. Song C, Liu Q, Zhi A, Yang J, Zhi Y, Li Q, et al. Development of a lateral flow colloidal gold immunoassay strip for the rapid detection of olaquindox residues. J Agric Food Chem. Sep. 2011;59(17):9319–26.
78. Jiang W, Liu Y, Chen Y, Yang Q, Chun P, Yao K, et al. A novel dynamic flow immunochromatographic test (DFICT) using gold nanoparticles for the serological detection of toxoplasma gondii infection in dogs and cats. Biosens Bioelectron. 2015;72:133–9.
79. Cvak B, Pum D, Molinelli A, Krska R. Synthesis and characterization of colloidal gold particles as labels for antibodies as used in lateral flow devices. Analyst. 2012;137(8):1882–7.
80. Chen YY, Tseng CW, Chang HY, Hung YL, Huang CC. Gold nanoparticle-based colorimetric assays for coagulation-related proteins and their inhibition reactions. Biosens Bioelectron. 2011;26(7):3160–6.

81. Petrakova AV, Urusov AE, Zherdev AV, Dzantiev BB. Gold nanoparticles of different shape for bicolor lateral flow test. *Anal Biochem*. 2019;568(August 2018):7–13.
82. Fu X, Chu Y, Zhao K, Li J, Deng A. Ultrasensitive detection of the β-adrenergic agonist brombuterol by a SERS-based lateral flow immunochromatographic assay using flower-like gold-silver core-shell nanoparticles. Microchim Acta. 2017;184(6):1711–9.
83. Parab HJ, Jung C, Lee JH, Park HG. A gold nanorod-based optical DNA biosensor for the diagnosis of pathogens. Biosens Bioelectron. Oct. 2010;26(2):667–73.
84. Mühlig S, Rockstuhl C, Yannopapas V, Bürgi T, Shalkevich N, Lederer F. Optical properties of a fabricated self-assembled bottom-up bulk metamaterial. *Opt Express*. 2011;19(10):9607.
85. Mayilo S, Kloster MA, Wunderlich M, Lutich A, Klar TA, Nichtl A, et al. Long-range fluorescence quenching by gold nanoparticles in a sandwich immunoassay for cardiac troponin T. Nano Lett. Dec. 2009;9(12):4558–63.
86. Cho IH, Bhunia A, Irudayaraj J. Rapid pathogen detection by lateral-flow immunochromatographic assay with gold nanoparticle-assisted enzyme signal amplification. Int J Food Microbiol. 2015;206:60–6.
87. Jauset-Rubio M, et al. Ultrasensitive, rapid and inexpensive detection of DNA using paper based lateral flow assay. *Sci Rep*. 2016;6(1):37732.
88. Koczula KM, Gallotta A. Lateral flow assays. Essays Biochem. 2016;60(1):111–20.
89. Si J, Li J, Zhang L, Zhang W, Yao J, Li T, et al. A signal amplification system on a lateral flow immunoassay detecting for hepatitis e-antigen in human blood samples. J Med Virol. Jul. 2019;91(7):1301–6.
90. Yetisen AK, Akram MS, Lowe CR. Paper-based microfluidic point-of-care diagnostic devices. Lab Chip. 2013;13(12):2210–51.
91. Harmsen S, Wall MA, Huang R, Kircher MF. Cancer imaging using surface-enhanced resonance Raman scattering nanoparticles. Nat Protoc. Jul. 2017;12(7):1400–14.
92. Quesada-González D, Stefani C, González I, de la Escosura-Muñiz A, Domingo N, Mutjé P, et al. Signal enhancement on gold nanoparticle-based lateral flow tests using cellulose nanofibers. Biosens Bioelectron. Sep. 2019;141:111407.
93. Bu T, et al. Diversely positive-charged gold nanoparticles based biosensor: a label-free and sensitive tool for foodborne pathogen detection. *Food Chem X*. 2019;3.
94. X. Yu, L. Wei, H. Chen, X. Niu, Y. Dou, and J. Yang, "Development of colloidal gold-based immunochromatographic assay for rapid detection of goose parvovirus," vol. 9, no. May, pp. 1–7, 2018.
95. Fu X, Cheng Z, Yu J, Choo P, Chen L, Choo J. A SERS-based lateral flow assay biosensor for highly sensitive detection of HIV-1 DNA. Biosens Bioelectron. Apr. 2016;78:530–7.
96. Pawade BS, Salvi NC, Shaikh IK, Waghmare AB, Jadhav ND, Wagh VB, et al. Rapid and selective detection of experimental snake envenomation – use of gold nanoparticle based lateral flow assay. Toxicon. Sep. 2016;119:299–306.
97. Urusov AE, Gubaidullina MK, Petrakova AV, Zherdev AV, Dzantiev BB. A new kind of highly sensitive competitive lateral flow immunoassay displaying direct analyte-signal dependence. Application to the determination of the mycotoxin deoxynivalenol. *Microchim Acta*. 2018;185(1):29.
98. Kumar R, Dilbaghi N, Kumar S, Gupta AK, Khurana SK, Yadav SC. Development of lateral flow assay for point-of-care diagnosis of trypanosomosis in equines. J Equine Vet Sci. 2018;70:1–6.
99. Dhanze H, Bhilegaonkar KN, Kumar C, Kumar MS, Singh P, Kumar A. Development and evaluation of lateral flow assay for sero-diagnosis of Japanese encephalitis in swine. Anim Biotechnol. 2019;0(0):1–7.
100. Choi DH, Lee SK, Oh YK, Bae BW, Lee SD, Kim S, et al. A dual gold nanoparticle conjugate-based lateral flow assay (LFA) method for the analysis of troponin I. Biosens Bioelectron. 2010;25(8):1999–2002.
101. Li J, Zou M, Chen Y, Xue Q, Zhang F, Li B, et al. Gold immunochromatographic strips for enhanced detection of avian influenza and Newcastle disease viruses. Anal Chim Acta. 2013;782:54–8.
102. Liu X, Xiang JJ, Tang Y, Zhang XL, Fu QQ, Zou JH, et al. Colloidal gold nanoparticle probe-based immunochromatographic assay for the rapid detection of chromium ions in water and serum samples. Anal Chim Acta. 2012;745:99–105.
103. Man Y, Lv X, Iqbal J, Peng G, Song D, Zhang C, et al. Microchip based and immunochromatographic strip assays for the visual detection of interleukin-6 and of tumor necrosis factor α using gold nanoparticles as labels. Microchim Acta. Feb. 2015;182(3–4):597–604.
104. Mdluli P, Tetyana P, Sosibo N, van der Walt H, Mlambo M, Skepu A, et al. Gold nanoparticle based tuberculosis immunochromatographic assay: the quantitative ESE Quanti analysis of the intensity of test and control lines. Biosens Bioelectron. 2014;54:1–6.
105. Meng K, Sun W, Zhao P, Zhang L, Cai D, Cheng Z, et al. Development of colloidal gold-based immunochromatographic assay for rapid detection of mycoplasma suis in porcine plasma. Biosens Bioelectron. May 2014;55:396–9.
106. Parolo C, de la Escosura-Muñiz A, Merkoçi A. Enhanced lateral flow immunoassay using gold nanoparticles loaded with enzymes. Biosens Bioelectron. 2013;40(1):412–6.
107. Preechakasedkit P, Pinwattana K, Dungchai W, Siangproh W, Chaicumpa W, Tongtawe P, et al. Development of a one-step immunochromatographic strip test using gold nanoparticles for the rapid detection of Salmonella typhi in human serum. Biosens Bioelectron. 2012;31(1):562–6.
108. Urusov AE, Petrakova AV, Kuzmin PG, Zherdev AV, Sveshnikov PG, Shafeev GA, et al. Application of gold nanoparticles produced by laser ablation for immunochromatographic assay labeling. Anal Biochem. 2015;491:65–71.
109. Wang X, Li Y, Wang H, Fu Q, Peng J, Wang Y, et al. Gold nanorod-based localized surface plasmon resonance biosensor for sensitive detection of hepatitis B virus in buffer, blood serum and plasma. Biosens Bioelectron. 2010;26(2):404–10.
110. Wen-de W, et al. Development of a colloidal gold immunochromatographic strip for rapid detection of *Streptococcus agalactiae* in tilapia. *Biosens Bioelectron*. 2017;91(2016):66–9.
111. Yang F, et al. Development of immunochromatographic test strips for rapid, quantitative detection of H9AIV antibodies. *J Chromatogr B Anal Technol Biomed Life Sci*. 2018;1095(July):59–64.
112. Li J, Duan H, Xu P, Huang X, Xiong Y. Effect of different-sized spherical gold nanoparticles grown layer by layer on the sensitivity of an immunochromatographic assay. RSC Adv. 2016;6(31):26178–85.
113. Ambrosi A, Airò F, Merkoçi A, Airò F, Merkoçi A. Enhanced gold nanoparticle based ELISA for a breast cancer biomarker. Anal Chem. 2010;82(3):1151–6.
114. Rodríguez MO, Covián LB, García AC, Blanco-López MC. Silver and gold enhancement methods for lateral flow immunoassays. Talanta. Feb. 2016;148:272–8.
115. J. T. Dias, G. Svedberg, M. Nystrand, H. Andersson-Svahn, and J. Gantelius, "Rapid signal enhancement method for nanoprobe-based biosensing," *Sci Rep*, vol. 7, no. 1, p. 6837, 2017.
116. Biagini RE, Sammons DL, Smith JP, MacKenzie BA, Striley CAF, Snawder JE, et al. Rapid, sensitive, and specific lateral-flow immunochromatographic device to measure anti-Anthrax protective antigen immunoglobulin G in serum and whole blood. Clin Vaccine Immunol. May 2006;13(5):541–6.

117. Du P, et al. A competitive bio-barcode amplification immunoassay for small molecules based on nanoparticles. *Sci Rep*. 2016;6(1): 38114.
118. Laderman EI, Whitworth E, Dumaual E, Jones M, Hudak A, Hogrefe W, et al. Rapid, sensitive, and specific lateral-flow immunochromatographic point-of-care device for detection of herpes simplex virus type 2-specific immunoglobulin G antibodies in serum and whole blood. Clin Vaccine Immunol. 2008;15(1): 159–63.
119. Thornton CR. Development of an immunochromatographic lateral-flow device for rapid serodiagnosis of invasive aspergillosis. Clin Vaccine Immunol. Jul. 2008;15(7):1095–105.
120. Tsai T-TT, Huang T-HH, Chen C-AC-FFCA, Ho NY-JJ, Chou Y-JJ, Chen C-AC-FFCA. Development a stacking pad design for enhancing the sensitivity of lateral flow immunoassay. Sci Rep. Dec. 2018;8(1):1–10.
121. Kikkas I, Mallone R, Larger E, Volland H, Morel N. A rapid lateral flow immunoassay for the detection of tyrosine phosphatase-like protein IA-2 autoantibodies in human serum. *PLoS One*. 2014;9(7):e103088.
122. Liu B, Wang L, Tong B, Zhang Y, Sheng W, Pan M, et al. Development and comparison of immunochromatographic strips with three nanomaterial labels: colloidal gold, nanogold-polyaniline-nanogold microspheres (GPGs) and colloidal carbon for visual detection of salbutamol. Biosens Bioelectron. 2016;85: 337–42.
123. Zhang G, Wang X, Zhi A, Bao Y, Yang Y, Qu M, et al. Development of a lateral flow immunoassay strip for screening of sulfamonomethoxine residues. Food Addit Contam Part A. Apr. 2008;25(4):413–23.
124. Byzova NA, Smirnova NI, Zherdev AV, Eremin SA, Shanin IA, Lei HT, et al. Rapid immunochromatographic assay for ofloxacin in animal original foodstuffs using native antisera labeled by colloidal gold. Talanta. Feb. 2014;119:125–32.
125. Di Nardo F, Baggiani C, Giovannoli C, Spano G, Anfossi L. Multicolor immunochromatographic strip test based on gold nanoparticles for the determination of aflatoxin B1 and fumonisins. Microchim Acta. May 2017;184(5):1295–304.
126. Pengsuk C, Chaivisuthangkura P, Longyant S, Sithigorngul P. Development and evaluation of a highly sensitive immunochromatographic strip test using gold nanoparticle for direct detection of Vibrio cholerae O139 in seafood samples. Biosens Bioelectron. 2013;42(1):229–35.
127. Rong-Hwa S, Shiao-Shek T, Der-Jiang C, Yao-Wen H. Gold nanoparticle-based lateral flow assay for detection of staphylococcal enterotoxin B. Food Chem. 2010;118(2):462–6.
128. Li Y-SS, et al. Development of a one-step test strip for rapid screening of fumonisins B1, B2 and B3 in maize. Food Control. 2012;24(1–2):72–7.
129. Urusov AE, Zherdev AV, Dzantiev BB. Use of gold nanoparticle-labeled secondary antibodies to improve the sensitivity of an immunochromatographic assay for aflatoxin B1. Microchim Acta. 2014;181(15–16):1939–46.
130. Wang Z, Guo L, Liu L, Kuang H, Xu C. Colloidal gold-based immunochromatographic strip assay for the rapid detection of three natural estrogens in milk. *Food Chem*. 2018;259(October 2017):122–9.
131. Lu S-YY, et al. A screening lateral flow immunochromatographic assay for on-site detection of okadaic acid in shellfish products. Anal Biochem. 2012;422(2):59–65.
132. Chen Y, Liu L, Xu L, Song S, Kuang H, Cui G, et al. Gold immunochromatographic sensor for the rapid detection of twenty-six sulfonamides in foods. Nano Res. Aug. 2017;10(8): 2833–44.
133. Yu CY, Ang GY, Chua AL, Tan EH, Lee SY, Falero-Diaz G, et al. Dry-reagent gold nanoparticle-based lateral flow biosensor for the simultaneous detection of Vibrio cholerae serogroups O1 and O139. J Microbiol Methods. 2011;86(3):277–82.
134. Shiu CM, Wang JJ, Yu FY. Sensitive enzyme-linked immunosorbent assay and rapid one-step immunochromatographic strip for fumonisin B1 in grain-based food and feed samples. J Sci Food Agric. 2010;90(6):1020–6.
135. Venkataramana M, Navya K, Chandranayaka S, Priyanka SR, Murali HS, Batra HV. Development and validation of an immunochromatographic assay for rapid detection of fumonisin B1 from cereal samples. J Food Sci Technol. Sep. 2014;51(9): 1920–8.
136. Ren W, Huang Z, Xu Y, Li Y, Ji Y, Su B. Urchin-like gold nanoparticle-based immunochromatographic strip test for rapid detection of fumonisin B1 in grains. Anal Bioanal Chem. 2015;407(24):7341–8.
137. Laura A, Gilda D, Claudio B, Cristina G, Gianfranco G. A lateral flow immunoassay for measuring ochratoxin a: development of a single system for maize, wheat and durum wheat. Food Control. 2011;22(12):1965–70.
138. Anfossi L, Baggiani C, Giovannoli C, Biagioli F, D'Arco G, Giraudi G. Optimization of a lateral flow immunoassay for the ultrasensitive detection of aflatoxin M1 in milk. Anal Chim Acta. 2013;772:75–80.
139. Naik L, Sharma R, Mann B, Lata K, Rajput YSS, Surendra Nath B. Rapid screening test for detection of oxytetracycline residues in milk using lateral flow assay. Food Chem. 2017;219:85–92.
140. Hua X, Qian G, Yang J, Hu B, Fan J, Qin N, et al. Development of an immunochromatographic assay for the rapid detection of chlorpyrifos-methyl in water samples. Biosens Bioelectron. Sep. 2010;26(1):189–94.
141. Kim YA, Lee EH, Kim KO, Lee YT, Hammock BD, Lee HS. Competitive immunochromatographic assay for the detection of the organophosphorus pesticide chlorpyrifos. Anal Chim Acta. 2011;693(1–2):106–13.
142. Wang L, Cai J, Wang Y, Fang Q, Wang S, Cheng Q, et al. A bare-eye-based lateral flow immunoassay based on the use of gold nanoparticles for simultaneous detection of three pesticides. Microchim Acta. Oct. 2014;181(13–14):1565–72.
143. Fu Q, Tang Y, Shi C, Zhang X, Xiang J, Liu X. A novel fluorescence-quenching immunochromatographic sensor for detection of the heavy metal chromium. Biosens Bioelectron. 2013;49:399–402.